ORIGINAL ARTICLE

Functional Segregation of the Human Dorsomedial Prefrontal Cortex

Simon B. Eickhoff[1,2], Angela R. Laird[3], Peter T. Fox[4], Danilo Bzdok[1,2], and Lukas Hensel[1]

[1]Institute of Neuroscience and Medicine (INM-1), Research Center Jülich, Jülich 52428, Germany, [2]Institute of Clinical Neuroscience and Medical Psychology, Heinrich Heine University, Düsseldorf 40225, Germany, [3]Department of Physics, Florida International University, Miami, FL 11200, USA, and [4]Research Imaging Institute, University of Texas Health Science Center, San Antonio, TX 7703, USA

Address correspondence to Dr Simon Eickhoff, Institut für Neurowissenschaften und Medizin (INM-1), 20, Forschungszentrum Jülich GmbH, D-52425 Jülich, Germany. Email: s.eickhoff@fz-juelich.de

Danilo Bzdok and Lukas Hensel contributed equally to this work.

Abstract

The human dorsomedial prefrontal cortex (dmPFC) has been implicated in various complex cognitive processes, including social cognition. To unravel its functional organization, we assessed the dmPFC's regional heterogeneity, connectivity patterns, and functional profiles. First, the heterogeneity of a dmPFC seed, engaged during social processing, was investigated by assessing local differences in whole-brain coactivation profiles. Second, functional connectivity of the ensuing dmPFC clusters was compared by task-constrained meta-analytic coactivation mapping and task-unconstrained resting-state correlations. Third, dmPFC clusters were functionally profiled by forward/reverse inference. The dmPFC seed was thus segregated into 4 clusters (rostroventral, rostrodorsal, caudal-right, and caudal-left). Both rostral clusters were connected to the amygdala and hippocampus and associated with memory and social cognitive tasks in functional decoding. The rostroventral cluster exhibited strongest connectivity to the default mode network. Unlike the rostral segregation, the caudal dmPFC was divided by hemispheres. The caudal-right cluster was strongly connected to a frontoparietal network (dorsal attention network), whereas the caudal-left cluster was strongly connected to the anterior midcingulate cortex and bilateral anterior insula (salience network). In conclusion, we demonstrate that a dmPFC seed reflecting social processing can be divided into 4 separate functional modules that contribute to distinct facets of advanced human cognition.

Key words: connectivity-based parcellation, default mode network, functional connectivity, lateralization, social cognition

Introduction

It is often claimed that the prefrontal cortex has expanded in volume in humans (cf. Bonin 1941; Passingham 1973) primarily to enable increasingly complex social behavior (cf. *social brain hypothesis*, Humphrey 1978; Dunbar and Shultz 2007). Recent evidence however paints a more complicated picture (cf. Semendeferi et al. 2002). Some evidence suggests that BA10 may be the only area larger in humans than great apes (Semendeferi et al. 2001; Petrides et al. 2012). The human prefrontal white-matter volume is also enlarged relative to its gray-matter volume (Schoenemann et al. 2005), especially in the language-dominant hemisphere (Smaers et al. 2011). From yet another perspective, increased gyrification (i.e., extent of cortical folding) of the prefrontal cortex might also set humans apart from monkeys as reported in cross-species comparisons of brain morphology (Rilling and Insel 1999). Consequently, the cognitive specialization of the human primate brain for maintaining sophisticated social

systems (Byrne and Whiten 1988; Dunbar 1998) goes hand in hand with a mosaic evolution and reorganization of the (medial) prefrontal cortex (Holloway 1968; Hoffman 2014).

Some findings have moreover drawn much interest to the more ventral portions of the medial prefrontal cortex (mPFC) as contributing to particularly advanced human cognition, including social cognition (cf. Amodio and Frith 2006; Mitchell 2009). Yet, a systematic review of the ventral versus dorsal aspects of the medial frontal lobe in social information processing based on lesion studies, experimental neuroimaging studies, and functional and structural connectivity highlighted the dorsomedial prefrontal cortex (dmPFC) as hierarchically higher and more tuned to processing uncertainty (Bzdok, Langner, Schilbach, Engemann, et al. 2013). Additionally, functional decoding revealed high-level social cognitive tasks to be more strongly associated with activation of the dorsal than ventral mPFC. In fact, the dmPFC was "the only" point of convergence in the whole brain when comparing neural activity selective for complex social judgments on visual face stimuli (Bzdok, Langner, et al. 2012) and on auditory voice stimuli (Hensel et al. forthcoming). This suggests that neural processing in the dmPFC reaches across sensory input channels and across different types of social judgments. Indicating a role extending beyond social cognition alone, coordinate-based meta-analyses of neuroimaging reports demonstrated that convergence of brain activity in the human frontal lobe was consistently "largest" in the dmPFC for not only social cognitive processes such as theory of mind (Spreng et al. 2009; Mar 2011) and moral reasoning (Bzdok, Schilbach, et al. 2012), but also "nonsocial" semantic processing (Binder et al. 2009) and autobiographical memory retrieval (Spreng et al. 2009). Importantly, as a key node within the default mode network, the dmPFC was also frequently observed during the absence of task (Raichle et al. 2001; Laird, Eickhoff, Li, et al. 2009). In sum, research based on disparate methods suggests the dmPFC to be one of the highest associative centers in the frontal lobe. It may moreover be particularly relevant for highly demanding and uniquely human social cognitive tasks.

It is important to appreciate that distinct parts of the dmPFC may be recruited by different high-level cognitive functions. More generally, the anatomical subdivisions of the entire human mPFC were first mapped out by Brodmann's cytoarchitectonic studies (Brodmann 1909). Later anatomical studies confirmed a "cytoarchitectonic segregation" within the mPFC in monkeys (Carmichael and Price 1994) and humans (Öngür et al. 2003). This evidence from different species together suggests that regional anatomical specialization in the mPFC enables regional "functional segregation." The cytoarchitectonical subdivision of the mPFC into BA 11 (orbitofrontal cortex), BA 10 (ventral mPFC and most of frontal pole), and BA 9 (dorsal mPFC and small part of frontal pole) might however not exhaustively capture local functional heterogeneity in that region. As a rare example in fMRI research, topographically distinct parts of the human dmPFC were recruited in neuroimaging contrasts of social, emotional, memory, and attentional tasks from independent neuroimaging studies (Gilbert, Henson, et al. 2010). This hints at a very fine-grained scale of functional specialization in the highly evolved dmPFC in humans. How the various functions converge or diverge with respect to their dmPFC representations, however, is currently largely unknown.

We therefore revisited the functional heterogeneity of the human dmPFC in high-level social cognition. Due to the lack of established anatomical boundaries of the dmPFC, we derived a seed region based on neural activation during social judgments across visual (Bzdok, Langner, et al. 2012) and auditory stimuli

(Hensel et al. forthcoming). First, we conducted connectivity-based parcellation (Johansen-Berg et al. 2004; Eickhoff et al. 2011) extracting meta-data from hundreds of previous imaging studies. This analysis tested whether regional differences in the dmPFC's whole-brain functional connectivity patterns enable identification of distinct subregions. Second, the ensuing connectivity-derived subregions in the dmPFC VOI were characterized by determining their brain-wide connectivity profiles based on 2 complementary measures of functional connectivity: Meta-analytic connectivity modeling (MACM) capturing brain activity in experimental settings and resting-state functional connectivity (RSFC) capturing brain activity outside of experimental constraints. This analysis tested what parts of the brain relate to the delineated subregions congruently in the presence and absence of defined psychological tasks. Third, we decoded the derived subregions' functional associations by correspondence with the extensive meta-data in the BrainMap database (Fox and Lancaster 2002) by means of forward and reverse inference. This last analysis tested whether subregions in the dmPFC are more robustly associated with particular types of paradigms or contrasts than would be expected by chance. Taken together, the present study should thus provide a statistically defensible characterization of subdivisions, connectivity, and functions associated with advanced social processing of the human dmPFC.

Materials and Methods

Defining the Volume of Interest

Since no anatomical boundaries have been established for the dmPFC, a "volume of interest" (VOI) for the current study was formed by combining contrast analyses from 2 prior neuroimaging studies. Both used functional magnetic resonance imaging (fMRI) to compare brain activity underlying complex social judgments (trustworthiness and attractiveness) with emotional (happiness) and cognitive (age) judgments. In the first study (Bzdok, Langner, et al. 2012) visually presented facial stimuli were evaluated, whereas auditorily presented vocal stimuli of everyday sentences were evaluated in the second study (Hensel et al. forthcoming). In both studies, we found brain activity exclusively related to social judgments by parceling out brain activity shared with emotional and cognitive judgments. Testing for topographical convergence between these 2 independent contrast analyses revealed the dmPFC as "the only" region that featured specific brain activity related to complex social judgments congruently across visual and auditory stimuli. Subsequent to sagittal mirroring for symmetry, this VOI reflecting the part of the dmPFC that was specifically recruited by complex social judgments provided the basis for all present analyses (Fig. 1).

Workflow

First, we quantitatively mapped the whole-brain coactivation profile of each voxel within the VOI using a range of neighborhood-filter sizes. The seed voxels were then grouped based on similarities of their coactivation profiles by k-means clustering. Following the selection of the most stable filter-size range, the optimal clustering solution was identified by the combination of different metrics for quantifying cluster stability. Second, the whole-brain connectivity patterns of each derived cluster (i.e., subregion within the VOI) were determined based on MACM and RSFC. Third, the functional patterns of the ensuing clusters were determined by significant overrepresentation of taxonomic classes of the BrainMap studies, which describe psychological

Figure 1. Volume of interest in the dmPFC. The volume of interest (VOI) in the dmPFC was previously identified as the only converging region between 2 neuroimaging studies on complex social judgments. Both studies contrasted complex social judgments to emotional and cognitive decisions based on visual faces (Bzdok, Langner, et al. 2012) and auditory voices (Hensel et al. forthcoming), respectively. The resulting seed region was sagittally mirrored for symmetry; the VOI was rendered into a T_1-weighted MNI single-subject template using Mango (http://ric.uthscsa.edu/mango/).

and experimental properties of each stored neuroimaging study (functional decoding).

Meta-analytic Connectivity Modeling

Delineation of whole-brain coactivation maps for each voxel of the dmPFC seed region was performed based on the BrainMap database (www.brainmap.org; Fox and Lancaster 2002; Laird et al. 2011). We constrained our analysis to fMRI and PET experiments from "normal mapping" neuroimaging studies (no interventions, no group comparisons) in healthy participants, which report results as coordinates in stereotaxic space. These inclusion criteria yielded ~7500 eligible experiments at the time of analysis. Please note that we considered all eligible BrainMap experiments because any preselection based on taxonomic categories would have constituted a strong a priori hypothesis about how brain networks are organized. However, it remains elusive how well psychological constructs, such as emotion and cognition, map on regional brain responses (Mesulam 1998; Poldrack 2006; Laird, Eickhoff, Kurth, et al. 2009).

The idea of the coactivation analysis is to compute the convergence across (all foci of) those BrainMap experiments where the seed voxel in question is reported as active (Laird et al. 2013). However, a challenge in constructing coactivation maps is the limited number of experiments activating precisely at a particular seed voxel. Hence, pooling across the close spatial neighborhood has become the dominant approach in MACM analysis (Cauda et al. 2011; Eickhoff et al. 2011). In the present study, we realized such pooling across a closely adjacent neighborhood, as needed to reliably determine the coactivation patterns of a given seed voxel, by identifying those among the ~7500 eligible experiments in BrainMap that reported closest activation to that voxel. That is, the experiments associated with each seed voxel were defined by activation at or in the immediate vicinity of this specific seed voxel. In particular, we calculated the respective Euclidean distances between the current seed voxel and individual foci of all database experiments to identify the 20 up to 200 experiments in steps of 2 (i.e., closest 20, 22, 24, . . . , 120 experiments) that feature the closest foci. The ensuing 51 experiment sets were then individually submitted to ALE meta-analysis to yield coactivation maps for the current seed voxel. A final coactivation map for each seed voxel was subsequently computed by their voxel-wise median. The seed voxels' final coactivation map indicates how likely voxels/areas throughout the brain are to increase metabolic activity concomitantly

with that seed voxel. This approach allows a robust and unbiased definition of coactivation patterns in spite of the variable and often rather low number of foci at each particular voxel. This was implemented by calculating and subsequently sorting the Euclidean distances between a given seed voxel and any activation reported in BrainMap. Then, the x nearest activation foci (i.e., filter size) were associated with that seed voxel.

The retrieved experiments were then used to compute the brain-wide coactivation profile of a given seed voxel for each of the 51 filter sizes. In particular, we performed a coordinate-based meta-analysis over all foci reported in these experiments to quantify their convergence. Since the experiments were identified by activation in or near a particular seed voxel, the highest convergence was evidently found at the location of the seed. Convergence outside the seed, however, indicated coactivation across task-based functional neuroimaging experiments.

These brain-wide coactivation patterns for each individual seed voxel were computed by activation likelihood estimation (ALE). The key idea behind ALE is to treat the foci reported in the associated experiments not as single points, but as centers for 3D Gaussian probability distributions that reflect the spatial uncertainty associated with neuroimaging results. Using the latest ALE implementation (Eickhoff et al. 2009, 2012; Turkeltaub et al. 2012), the spatial extent of those Gaussian probability distributions was based on empirical estimates of between-subject and between-template variance of neuroimaging foci (Eickhoff et al. 2009). For each experiment, the probability distributions of all reported foci were then combined into a modeled activation (MA) map by the recently introduced "nonadditive" approach that prevents local summation effects (Turkeltaub et al. 2012). The voxel-wise union across the MA maps of all experiments associated with the current seed voxel then yielded an ALE score for each voxel of the brain that describes the coactivation probability of that particular location with the current seed voxel. The ALE scores of all voxels within gray matter (based on 10% probability according to the ICBM maps) were recorded before moving to the next voxel of the seed region.

In sum, quantitative ALE meta-analysis over all foci reported in the experiments associated with the current seed voxel determined how likely any other voxel throughout the brain was to coactivate with that particular seed voxel. Please note that no threshold was applied to the ensuing coactivation maps at this point of analysis to retain the complete pattern of coactivation likelihood (cf. Bzdok, Langner, Schilbach, Jakobs, et al. 2013; Cieslik et al. 2013).

Connectivity-Based Parcellation

The unthresholded brain-wide coactivation profiles for all seed voxels were then combined into a $N_S \times N_T$ coactivation matrix, where N_S denotes the number of seed voxels (1310 voxels in the present VOI at $2 \times 2 \times 2$ mm³ resolution) and N_T the number of target voxels in the gray matter of the reference brain volume at $4 \times 4 \times 4$ mm³ resolution (~36 000 voxels located within gray matter). Given the use of 51 different filter sizes, this step resulted in 51 individual coactivation matrices, each representing the whole-brain connectivity of the seed voxels at a particular filter size. The parcellation of the VOI was performed using k-means clustering as implemented in Matlab with $K = 2, 3, \ldots, 5$ using one minus the correlation between the connectivity patterns of seed voxels as a distance's measure (i.e., correlation distance). This parcellation was performed for each of the 51 filter sizes independently, yielding 4 (k means cluster solutions) × 51 (filter size) independent cluster solutions (cf. Clos et al. 2013). K-means clustering is a nonhierarchical clustering method that uses an iterative algorithm to separate the seed region into a previously selected number of k nonoverlapping clusters (Forgy 1965; Hartigan and Wong 1979). K-means aims at minimizing the variance between elements within clusters and maximizing the variance between clusters by first computing the centroid of each cluster and subsequently reassigning voxels to the clusters such that their difference from the nearest centroid is minimal. For each of the 4×51 parcellations we recorded the best solutions from 100 replications with randomly placed initial centroids.

Selection of Optimal Filter Range

For each of the 51 filter sizes (i.e., seed-voxel-wise connectivity profiles based on different parameter choices regarding the number of voxel-associated experiments from the database), the k-means procedure thus yielded 4 different solutions of parcellating the dmPFC by subdivision into 2, 3, . . . , and 5 clusters. The challenge to identify the "optimal" cluster solution is thus further complicated in the current MACM-based parcellation approach because not only the optimal number of clusters k (i.e., how many subregions in the dmPFC) but also the spatial filter size (i.e., how many database experiments contribute to a seed voxel's connectivity map) had to be determined. In previous parcellation studies, using MACM, these 2 free parameters were reduced to a single one by "averaging across all filter sizes" (Bzdok, Laird, et al. 2012; Cieslik et al. 2013). As an improvement of this previous approach, we here used a recently introduced two-step procedure that involves a first decision on those filter sizes (i.e., the target range of voxel-wise connectivity profiles from x to y-associated experiments) to be included in the final analysis and a second decision on the optimal cluster solution (Clos et al. 2013). That is, we first examined the properties of each filter size across all cluster solutions and isolated "the most stable range of filter sizes." These were then submitted to further analysis selecting the number of clusters. The first step was based on the consistency of the cluster assignments for the individual voxels across the different filter sizes and selecting the filter range with the lowest number of deviants, that is, voxels that were assigned differently when compared with the solution from the majority (mode) of filters. In other words, we identified those filter sizes that reflected solutions most similar to the consensus solution. Comparing the number of deviant cluster assignments (i.e., the number of times a given voxel was assigned to another than the majority cluster; normalized for K) indicated that most deviants were present in parcellations based on small but also very large filter sizes. The filter-size range was set from

36 to 96. This was based on the increase in weighted sum (across all K) of the z-normalized number of deviant voxel assignments before and after these values. That is, at the cutoff at $z < -0.5$, only those filter sizes were included where the number of deviants was at least half a standard deviation below the average number of deviants across all filter sizes. This approach avoids a subjective choice on a particular single filter size and provides a quantitatively justified selection of the first parameter (filter sizes). In the subsequent step addressing the choice of the second parameter (number of clusters), all analyses were then restricted to the selected filter sizes.

Selection of the Optimal Number of Clusters

We subsequently determined "the optimal solution of K clusters" (restricted to the 51 selected filter sizes as outlined in the last paragraph). The "true" number of clusters is unknown for most real-world clustering problems, including neurobiological research. Finding an "optimal" number of clusters is widely acknowledged to be an unresolved issue (cluster validity problem) in computer science, pattern recognition, machine learning, and beyond (Jain et al. 1999; Handl et al. 2005). The absence of a mathematically perfect solution (Tibshirani et al. 2001) prompted the development of a diversity of cluster validity criteria to weigh the quality of obtained cluster solutions. In the present study, the choice of the k was therefore indicated by majority vote of 4 different criteria describing information-theoretic, cluster separation, and topological properties of the various cluster solutions.

First, as an information-theoretic criterion, we assessed the similarity of cluster assignments for each filter size between the current solution (K) and the neighboring solutions ($K - 1$ and $K + 1$) by using the variation of information (VI) metric (Meila 2007). The VI metric has been previously used for selecting the best fitting K-means parcellation model of a given brain region by Kelly et al. (2010) and Kahnt et al. (2012). The VI between 2 cluster solutions C and C' was computed by

$$\mathrm{VI}(C, C')_k = H(C)_k + H(C')_k - 2I(C, C')_k$$

where H represents the amount of information (entropy) present in the cluster solutions C and C', respectively, and I is the mutual information shared by the 2 cluster solutions C and C'. For each filter size, the VI metric was computed between a given K solution and the subsequent $K + 1$ solution. Solutions were considered stable either if there was an increase in VI from the current to the subsequent set of solutions (primary criterion) or if there was a decrease from the previous to the current clustering step (secondary criterion).

Second, as a cluster separation criterion, the silhouette coefficient (Kaufman and Rousseeuw 1990) is a general measure of how similar a given voxel is to voxels in its own cluster compared with voxels in other clusters (averaged across voxels of a filter size). This value ranges from -1 to $+1$. Good solutions are those with a higher silhouette value compared with the $K - 1$ solution (primary criterion) or whose silhouette coefficient is at least not decreased compared with the previous $K - 1$ solution (secondary criterion).

Third, as a topological criterion, we assessed the percentage of voxels not related to the dominant parent cluster compared with the $K - 1$ solution. This measure is related to the hierarchy index (Kahnt et al. 2012) and corresponds to the percentage voxels that are not present in hierarchy, K, compared with the previous $K - 1$ solution. That is, voxels assigned, for example, to the

blue cluster in the $K = 3$ solution stemming from a subset of voxels previously assigned to the green cluster (in the $K = 2$ solution) would be excluded if the majority of the blue cluster voxels actually stemmed from the red cluster (in the $K = 2$ solution). "Good solutions" for a given K cluster parcellation were those wherein the percentage of lost voxels was below the median across all possible solutions (cluster parcellations 2–5), where the respective clustering step resulted in a local minimum and/or the following clustering step featured a maximum in the percentage of lost (hierarchically inconsistent) voxels.

Fourth, as a consistency criterion, we considered the percentage of misclassified voxels (deviants) across-filter sizes of a given cluster solution. This criterion indirectly reflects the amount of noise and potentially local effects in the clustering. In particular, the criterion addresses the across-filter stability, that is, the average percentage of voxels for each filter size that were assigned to a different cluster compared with the most frequent assignment of these voxels across all filter sizes. Those K parcellations were considered good solutions whose percentages of deviants (presumably reflecting noise and local variance) were not increased compared with the $K − 1$ solution and, in particular, if the subsequent $K + 1$ solution lead to a higher percentage of deviants.

These different criteria estimating cluster stability conjointly allowed for an investigator-independent, cross-confirmed identification of the cluster solution indicating the highest within-cluster homogeneity and between-cluster heterogeneity. In other words, they identified the parcellation of the dmPFC that was most supported by the similarities and differences of the seed-voxel-wise whole-brain connectivity profiles.

Characterization of the Clusters: Task-Dependent Connectivity

To determine the significant functional connectivity of the derived "clusters," another MACM was performed. In the first step, we identified all experiments in the BrainMap database that featured at least one focus of activation in a particular cluster (derived from the coactivation-based parcellation). That is, in contradistinction to the above MACM analyses, we did not select experiments activating at or close to a particular voxel but rather all those that activated in one of the CBP-derived clusters. Next, an ALE meta-analysis was performed on these experiments as described above.

In contrast to the MACM underlying the coactivation-based parcellation, where ALE maps were not thresholded to retain the complete pattern of coactivation likelihoods, statistical inference was now performed. To establish which regions were significantly coactivated with a given cluster, ALE scores for the MACM analysis of this cluster were compared with a null-distribution reflecting a random spatial association between experiments with a fixed within-experiment distribution of foci (Eickhoff et al. 2009). This random-effects inference assesses above-chance convergence between experiments, not clustering of foci within a particular experiment. The observed ALE scores from the actual meta-analysis of experiments activating within a particular cluster were then tested against ALE scores obtained under a null-distribution of random spatial association yielding a P-value based on the proportion of equal or higher random values (Eickhoff et al. 2012). The resulting nonparametric P-values were transformed into Z-scores and thresholded at a cluster-level corrected threshold of $P < 0.05$ (cluster-forming threshold at voxel-level $P < 0.001$).

Differences in coactivation patterns between the identified clusters were tested by performing MACM separately on the

experiments associated with either cluster and computing the voxel-wise difference between the ensuing ALE maps. All experiments contributing to either analysis were then pooled and randomly divided into 2 groups of the same size as the 2 original sets of experiments defined by activation in the first or second cluster (Eickhoff et al. 2011). ALE scores for these 2 randomly assembled groups, reflecting the null-hypothesis of label-exchangeability, were calculated and the difference between these ALE scores was recorded for each voxel in the brain. Repeating this process 10 000 times then yielded a voxel-wise null-distribution on the differences in ALE scores between the MACM analyses of the 2 clusters. The "true" differences in ALE scores were then tested against this null-distribution yielding a P-value for the difference at each voxel based on the proportion of equal or higher differences under label-exchangeability. The resulting P-values were thresholded at $P > 0.95$ (95% chance of true difference), transformed into Z-scores, and inclusively masked by the respective main effects, that is, the significant effects in the MACM for the particular cluster.

Finally, we computed the specific coactivation pattern for all clusters, that is, brain regions significantly more coactivated with a given cluster than with any of the other ones. This specific cluster-wise coactivation pattern was computed by performing a conjunction analysis over the differences between this cluster and the remaining clusters.

Characterization of the Clusters: Task-Independent Connectivity

Significant cluster-wise whole-brain connectivity was likewise assessed using resting-state correlations as an independent modality of functional connectivity for cross-confirmation across disparate brain states. RSFC fMRI images were obtained from the Nathan Kline Institute "Rockland" sample, which are available online as part of the International Neuroimaging Datasharing Initiative (http://fcon_1000.projects.nitrc.org/indi/pro/nki.html). In total, the processed sample consisted of 132 healthy subjects between 18 and 85 years (mean age: 42.3 ± 18.08 years; 78 males, 54 females) with 260 echo-planar imaging (EPI) images per subject. Images were acquired on a Siemens TrioTim 3 T scanner using blood oxygen level–dependent (BOLD) contrast [gradient-echo EPI pulse sequence, repetition time (TR) = 2.5 s, echo time (TE) = 30 ms, flip angle = 80°, in-plane resolution = 3.0 × 3.0 mm, 38 axial slices (3.0 mm thickness), covering the entire brain]. The first 4 scans served as dummy images allowing for magnetic field saturation and were discarded prior to further processing using SPM8 (www.fil.ion.ucl.ac.uk/spm). The remaining EPI images were then first corrected for head movement by affine registration using a two-pass procedure. The mean EPI image for each participant was spatially normalized to the MNI single-subject template (Holmes et al. 1998) using the "unified segmentation" approach (Ashburner and Friston 2005) and the ensuing deformation was applied to the individual EPI volumes. Finally, images were smoothed by a 5-mm FWHM Gaussian kernel to improve signal-to-noise ratio and account for residual anatomical variations.

The time-series data of each individual seed voxel were processed as follows (Zu Eulenburg et al. 2012; Satterthwaite et al. 2013): To reduce spurious correlations, variance that could be explained by the following nuisance variables was removed: 1) The 6 motion parameters derived from the image realignment, 2) the first derivative of the realignment parameters, and 3) mean gray matter, white matter, and CSF signal per time point as obtained by averaging across voxels attributed to the respective tissue

class in the SPM 8 segmentation (Reetz et al. 2012). All of these nuisance variables entered the model as first-order and also as second-order terms (Jakobs et al. 2012). Data were then band-pass filtered preserving frequencies between 0.01 and 0.08 Hz since meaningful resting-state correlations will predominantly be found in these frequencies given that the BOLD-response acts as a low-pass filter (Biswal et al. 1995; Fox and Raichle 2007).

To measures cluster-wise task-independent connectivity, time courses were extracted for all gray-matter voxels of a given cluster. The cluster time course was then expressed as the first eigenvariate of these voxels' time courses. Pearson correlation coefficients between the time series of the CBP-derived dmPFC clusters and all other gray-matter voxels in the brain were computed to quantify RSFC. These voxel-wise correlation coefficients were then transformed into Fisher's Z-scores and tested for consistency in a flexible factorial model across subjects. The main effect of connectivity for individual clusters and contrasts between those were tested using the standard SPM8 implementations with the appropriate nonsphericity correction. Results were cluster-level thresholded at $P < 0.05$ (cluster-forming threshold at voxel-level: $P < 0.001$), analogous to the MACM-based difference analysis. The "specific" resting-state correlations for a given cluster were then computed by performing a conjunction analysis over the differences between this cluster and the remaining clusters, analogous to the MACM-based cluster analyses above.

Characterization of the Clusters: Conjunction across Connectivity Types and Clusters

To delineate areas showing task-dependent and task-independent functional connectivity with the derived subregions in the dmPFC, we performed a conjunction analysis of the MACM and RSFC results using the strict minimum statistics (Nichols et al. 2005; Rottschy et al. 2013).

Regions connected with "individual clusters" in both connectivity modalities were delineated by computing the intersection of the (cluster-level family-wise-error corrected) connectivity maps from the 2 connectivity analyses detailed above. In this way, each dmPFC cluster is associated with a network of areas that are congruently connected to that cluster across 2 disparate brain states, that is, task-focused and mind-wandering cognitive sets.

Characterization of the Clusters: Function

Finally, the identified clusters were individually submitted to functional decoding (Balsters et al.2014; Muller et al. 2014; Amft et al. forthcoming). Please note that this functional characterization constitutes a post hoc procedure that is subsequent to and independent of the connectivity analyses. The functional characterization was based on the BrainMap meta-data that describe each neuroimaging experiment included in the database. Behavioral domains code the mental processes isolated by the statistical contrasts (Fox, Laird, et al. 2005) and comprise the main categories cognition, action, perception, emotion, and interoception, as well as their related subcategories. Paradigm classes categorize the specific task employed (see http://brainmap.org/scribe/ for the complete BrainMap taxonomy).

"Forward inference" on the functional characterization tests the probability of observing activity in a brain region given knowledge of the psychological process, whereas "reverse inference" tests the probability of a psychological process being present given knowledge of activation in a particular brain region. In the forward inference approach, a cluster's functional profile was determined by identifying taxonomic labels for which the probability of finding activation in the respective cluster was significantly higher than the a priori chance (across the entire database) of finding activation in that particular cluster. Significance was established using a binomial test ($P < 0.05$). That is, we tested whether the conditional probability of activation given a particular label [P(Activation|Task)] was higher than the baseline probability of activating the region in question per se [P(Activation)]. In the reverse inference approach, a cluster's functional profile was determined by identifying the most likely behavioral domains and paradigm classes given activation in a particular cluster. This likelihood P(Task|Activation) can be derived from P(Activation|Task) as well as P(Task) and P(Activation) using Bayes' rule. Significance was then assessed by means of a χ^2 test ($P < 0.05$). In sum, forward inference assessed the probability of activation given a psychological term, while reverse inference assessed the probability of a psychological term given activation.

In the context of quantitative functional decoding, it is important to appreciate that this approach aims at relating defined psychological tasks to the examined brain regions instead of claiming "a unique role" of a brain region for any psychological task (Poldrack 2006; Yarkoni et al. 2011). Put differently, an association of task X to brain region Y obtained in these analyses does not necessarily imply that neural activity in region Y "is limited to" task X.

Anatomical Localization

The SPM Anatomy Toolbox (Eickhoff et al. 2005, 2007) was used to allow for investigator-independent anatomical localization of imaging results. By means of maximum probability maps (MPMs), activation clusters were automatically assigned to the most likely cytoarchitectonic area. MPMs are drawn from earlier microscopic investigations, including the intersubject variability and aided by algorithmic definition of microanatomical borders of brain areas (Zilles and Amunts 2010). Please note that not all areas have yet been cytoarchitectonically mapped. Not all activation clusters could thus be assigned to a cytoarchitectonic map.

Results

Parcellation

To determine the optimal parcellation of the dmPFC VOI, metrics quantified model fit for comparison between cluster solutions (Fig. 2). Information-theoretic, cluster separation, topological, and consistency criteria agreed in favoring the four-cluster solution as featuring the highest stability. First, the information-theoretic criterion indicated VI to decrease from 3 to 4 clusters and to increase toward 5 clusters. This minimum of variation thus reflected highest integrity of information in the four-cluster solution. Second, as cluster separation criterion, the silhouette coefficient showed an increase from 3 to 4 clusters, whereas this metric decreased again in 5 clusters. Four clusters thus exhibited highest similarity among the voxels in each cluster. Third, as topological criterion, the percentage of voxels not related to the dominant parent cluster was minimal in the four-cluster solution. Four clusters thus contained the least amount of regrouped voxels and therefore highest continuity with their dominant parent cluster from the $k - 1$ solution. Comparing to the three- and five-cluster solutions, the four-cluster solution showed highest hierarchical consistency. Fourth, as a consistency criterion, the percentage of misclassified voxels decreased in the four-cluster solution, whereas 5 clusters lost across-filter

stability. In sum, these 4 criteria measuring model fit all favored the four-cluster solution as the most stable segregation of the dmPFC VOI (Fig. 3).
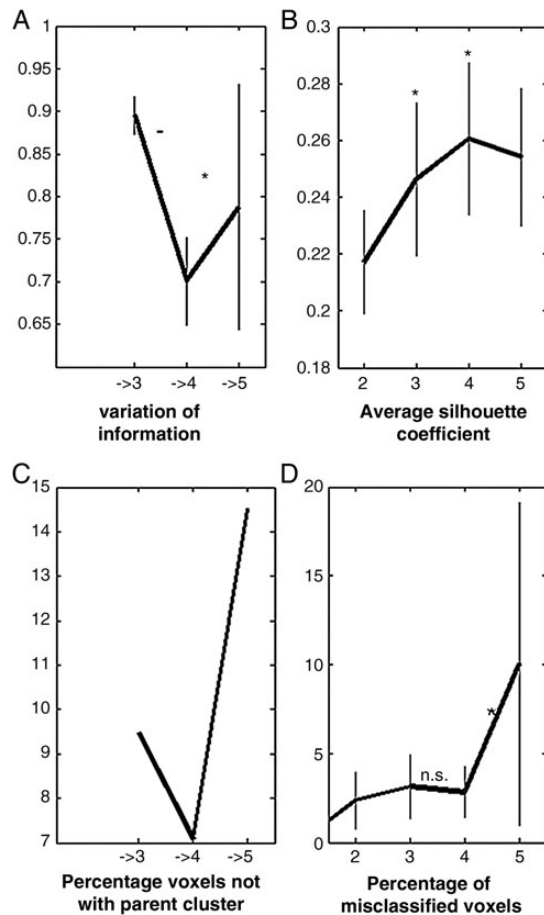

Figure 2. Cluster criteria for model selection. Four different criteria for model fit indicated highest stability in the four-cluster parcellation. (A) Variation of information decreased from 3 to 4 clusters and increased in a five-cluster solution. (B) The average silhouette coefficient rose with the number of clusters up to a maximum with 4 clusters. (C) The percentage of voxels not related to the dominant parent cluster was lowest with 4 clusters. (D) The percentage of misclassified voxels decreased at for clusters, before becoming unstable at the five-cluster solution. Thus, information-theoretic, cluster separation, and topological criteria identified the four-cluster solution as the best fitting model.
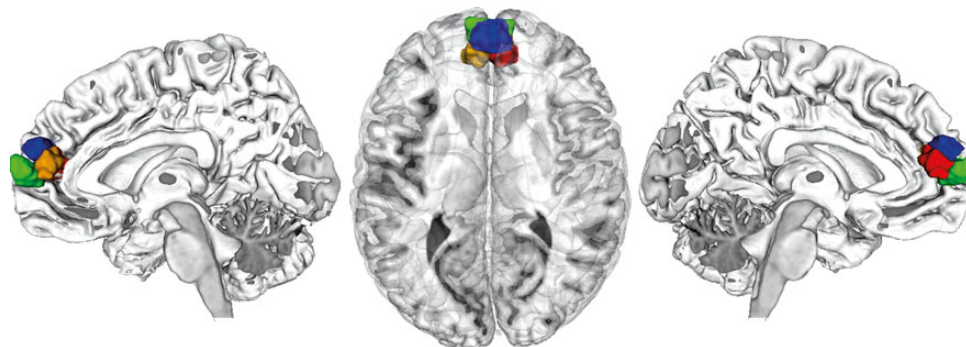
Individual Cluster Connectivity

To characterize each individual dmPFC cluster's functional connectivity, cluster-level corrected meta-analytic coactivations (MACM) were assessed for the 4 individual clusters (Fig. 4, top). The rostroventral (green), rostrodorsal (blue), and caudal-left (yellow) clusters coactivated with the ventromedial prefrontal cortex (vmPFC), anterior cingulate cortex (ACC), posterior cingulate cortex (PCC), left inferior parietal cortex [IPC; areas PGp and PGa (Caspers et al. 2006)], inferior frontal gyrus (IFG), amygdala, and hippocampus (for medial temporal cytoarchitectonic allocations, please see Table 1). Despite this partially overlapping connectivity pattern, several differences between clusters were observed: The left IFG was connected to the rostroventral green cluster, the rostrodorsal blue cluster, and the caudal-left yellow cluster, but coactivations of the rostrodorsal and caudal-left clusters extended substantially further into the left anterior insula. Additionally, only the caudal-left yellow cluster was connected to the anterior midcingulate cortex predominantly in the left hemisphere (aMCC; Vogt 2005). With respect to medial temporal connectivity, the caudal-left yellow cluster mainly coactivated with the left amygdalar laterobasal nuclei group (LB; Amunts et al. 2005), whereas the 2 rostral clusters (green and blue) were more connected to the amygdalar superficial nuclei group (SF; Amunts et al. 2005) and the left hippocampus (Table 1). In the right hemisphere, only the rostrodorsal blue cluster was significantly connected to the right amygdalar SF. This cluster further coactivated with the right extrastriate area V5 (hOc5; Malikovic et al. 2007). In contrast, only the rostroventral green cluster showed bilateral connectivity to IPC (bilateral areas PGp, left area PGa) and featured largest coactivations with vmPFC and PCC. Connectivity to all of the above-mentioned regions was absent for the caudal-right red cluster. Instead, the red cluster only coactivated with the left superior frontal sulcus (SFS). The rostroventral (green), rostrodorsal (blue), and caudal-left (yellow) clusters were also connected to the SFS, but in distinct, more rostral regions extending to the adjacent superior frontal gyrus (SFG).

After this assessment of task-dependent connectivity, we also determined the task-independent, RSFC for each individual cluster (Fig. 4, middle). Compared with the MACM analyses, RSFC yielded more extensively distributed connectivity patterns, although both analyses (MACM and RSFC) were cluster-level corrected at the same threshold of $P < 0.05$. All 4 clusters were connected to large frontal regions including bilateral vmPFC, OFC, frontal pole, SFG, SFS, IFG (area 45 in the left hemisphere; Amunts et al. 1999), ACC, MCC, and the precentral gyri (areas 4a, 4p; Geyer et al. 1996; and 6; Geyer 2004). The similarly extensive parietal connections of all clusters included bilateral PCC,
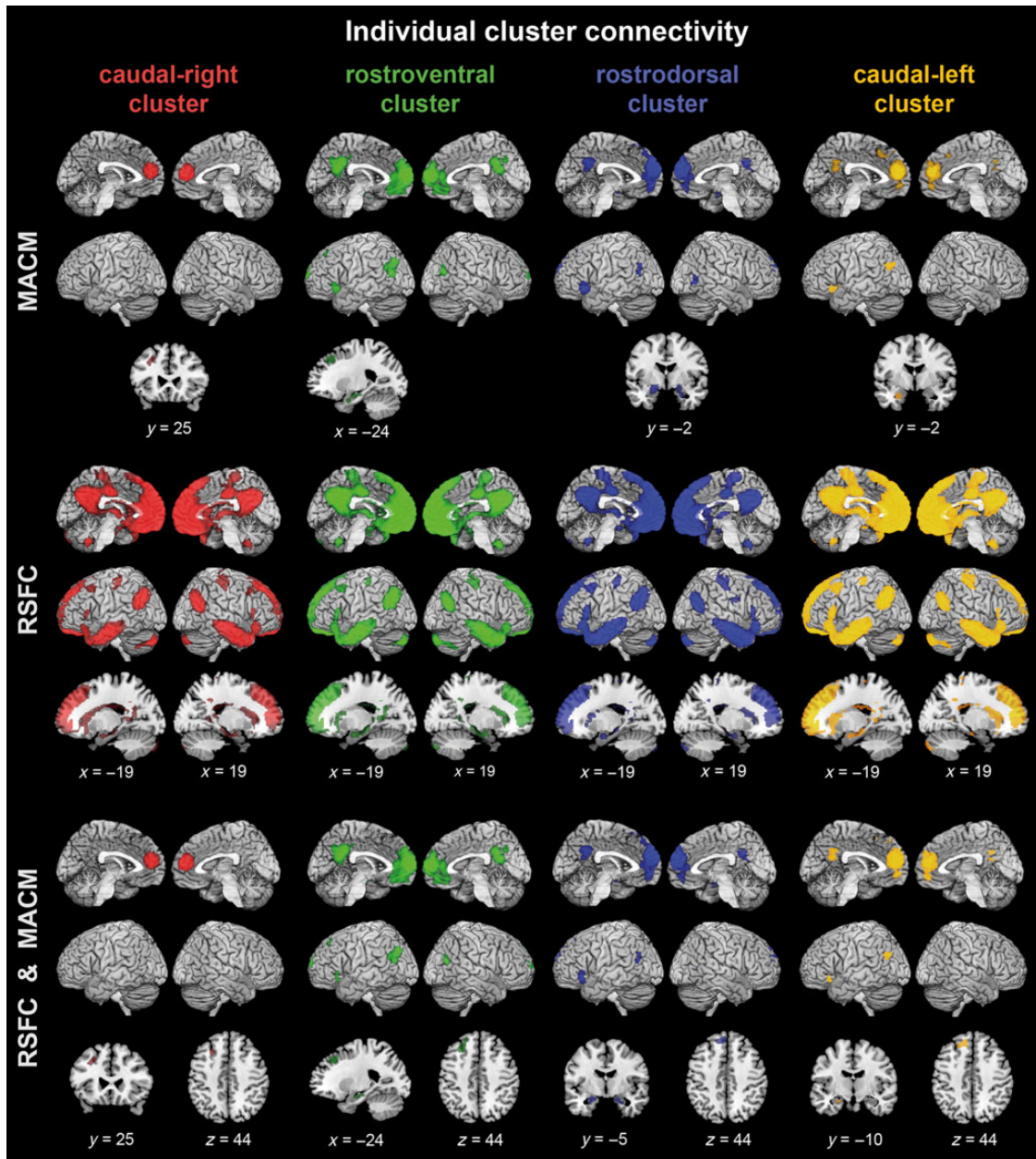

Figure 3. Connectivity-based parcellation results. Connectivity-based parcellation divided the dmPFC VOI into 4 connectionally homogeneous subregions, a caudal-right (red), rostroventral (green), rostrodorsal (blue), and caudal-left cluster (yellow). The results were rendered into a T_1-weighted MNI single-subject template using Mango.

Figure 4. Connectivity of the individual dmPFC clusters. Functional connectivity profiles of each dmPFC cluster based on meta-analytic connectivity modeling (MACM; top rows), resting-state functional connectivity (RSFC; middle rows), and the conjunction of RSFC and MACM results (RSFC and MACM; bottom rows). All results were cluster-level corrected at $P < 0.05$. All images were rendered into a T_1-weighted MNI single-subject template using MRIcron (http://www.nitrc.org/projects/mricron/).

precuneus, central sulci and postcentral gyri (areas 1, 3a, and 3b; Geyer et al. 1999), parietal opercula (areas OP2 and OP3; Eickhoff et al. 2006), superior parietal lobes (area 7M; Scheperjans et al. 2008), and IPC (bilateral PGa. PGp, and left PFm; Caspers et al. 2006). Furthermore, all clusters featured connectivity to bilateral middle frontal gyrus and inferior frontal gyri and the cerebellum (lobule VIIa crus I and II; Diedrichsen et al. 2009). Subcortically, connectivity of the clusters was commonly found in the bilateral thalami, caudate nuclei, hippocampi (cornu ammonis, fascia dentata, and subiculum; Amunts et al. 2005), and the left amygdala (LB and SF). Only the caudal-right (red), rostroventral (green), and rostrodorsal (blue) clusters were connected to the right amygdala (SF, rostroventral, and -dorsal clusters also LB). Notably, although all clusters were also connected to the left

dorsolateral prefrontal cortex (dlPFC), only the red cluster showed right-hemispheric dlPFC connectivity.

After the separate characterization of functional connectivity in task and rest, each clusters' congruent connectivity across both the presence (MACM) and absence (RSFC) of task was investigated by a conjunction analysis (cf. Materials and Methods, Fig. 4, bottom). Congruent connectivity of the rostroventral green cluster, the rostrodorsal blue cluster, and the caudal-left yellow cluster included bilateral vmPFC, the adjacent ACC, the PCC as well as left IPC (left area PGp, extending into PGa especially for the rostroventral green cluster), and IFG. In the medial temporal lobe, congruent effects confirmed the rostroventral green and rostrodorsal blue clusters' connectivity to LB, SF (amygdala), and the cornu ammonis (hippocampus), whereas

Table 1 Quantified topographical overlap of individual clusters' task-dependent connectivity pattern (MACM) with cytoarchitectonic maps in the left medial temporal lobe (congruent MACM and RSFC connectivity added in brackets)

	Rostroventral cluster (green)	Rostrodorsal cluster (blue)	Caudal-left cluster (yellow)
Left amygdala			
Connectivity overlap with SF	**20.30% (22.20%)**	**33.50% (27.10%)**	2.70% (8.70%)
Connectivity overlap with CM	1.20% (0.10%)	2.50% (0.10%)	0.10% (0.00%)
Connectivity overlap with LB	**33.70% (17.70%)**	**22.90% (36.20%)**	**85.00% (51.00%)**
SF overlap with connectivity	22.90% (12.60%)	**54.20% (18.80%)**	1.60% (0.60%)
CM overlap with connectivity	4.90% (0.10%)	14.20% (0.20%)	0.20% (0.00%)
LB overlap with connectivity	**23.60% (6.20%)**	**22.90% (15.50%)**	**30.40% (2.10%)**
Left hippocampus			
Connectivity overlap with HATA	1.80% (0.00%)	0.40% (0.00%)	0.00% (0.00%)
Connectivity overlap with CA	**25.60% (42.80%)**	**15.10% (33.90%)**	5.20% (29.80%)
Connectivity overlap with SUB	4.60% (8.40%)	0.40% (0.80%)	0.00% (0.00%)
HATA overlap with connectivity	**71.10% (0.00%)**	**22.20% (0.00%)**	0.00% (0.00%)
CA overlap with connectivity	7.20% (6.00%)	6.10% (5.80%)	0.70% (0.50%)
SUB overlap with connectivity	2.00% (1.80%)	0.20% (0.20%)	0.00% (0.00%)

Using the SPM Anatomy Toolbox (Eickhoff et al. 2005), we tested for topographic overlap of clusters' coactivations with probabilistic cytoarchitectonic maps of the amygdala and hippocampus (Amunts et al. 2005). The table exhibits left-hemispheric results only, since only the rostrodorsal cluster (blue) featured connectivity with the right medial temporal lobe (predominantly SF). Please note that the caudal-right cluster (red) did not show any significant meta-analytic connectivity to the medial temporal lobes. Anterior dmPFC clusters (green and blue) showed most robust coactivation with left hippocampus and amygdalar SF and LB. The caudal-left cluster (yellow) predominantly connected with left LB. Bold for visual accessibility.
SF, superficial nuclei group; CM, centromedial nuclei group; LB, laterobasal nuclei group; CA, cornu ammonis; SUB, subiculum.
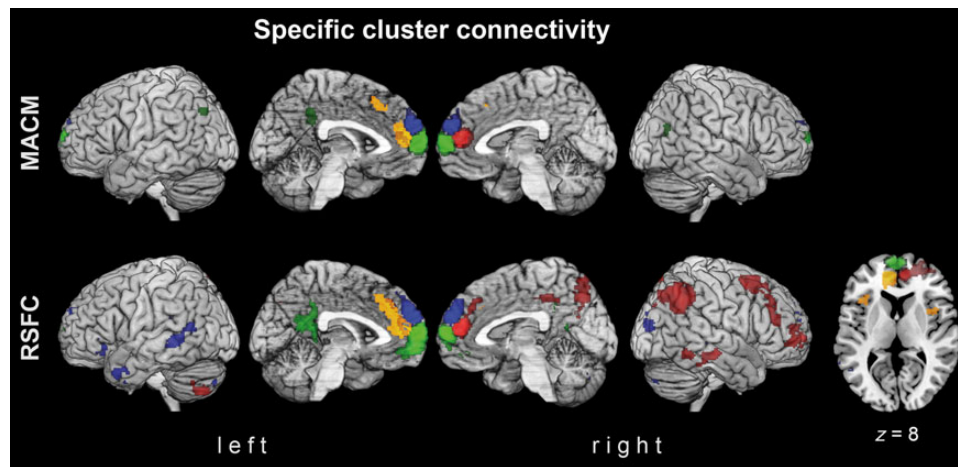

Figure 5. Specific connectivity of the individual dmPFC clusters. Depicting connectivity patterns which are stronger connected to a given dmPFC cluster, compared with all 3 other clusters based on meta-analytic connectivity modeling (MACM; top row) and resting-state functional connectivity (RSFC; middle row). Specific connectivity is rendered for caudal-right (red), rostroventral (green), rostrodorsal (blue), and caudal-left (yellow) cluster. All images were rendered into a T_1-weighted MNI single-subject template using MRIcron.

the caudal-left yellow cluster was predominantly connected to the amygdalar LB (Table 1). In the right hemisphere, additional congruent connectivity to the IPC (right area PGp) was found for the rostroventral green cluster, whereas the right amygdala (mostly SF) was congruently connected to the rostrodorsal blue cluster. The caudal-right red cluster was congruently connected to the left SFS, located posteriorly to SFS and SFG connectivity of the rostral green and blue clusters as well as the caudal-left yellow cluster.

Specific Cluster Connectivity

Due to the large similarity of functional connectivity of the dmPFC clusters (apart from the red cluster), a subsequent analysis targeted those brain regions that are more strongly connected to a given dmPFC cluster than the respective 3 other clusters (Fig. 5). To isolate these regions for one cluster, its functional connectivity was contrasted to those of all other clusters in 3 separate comparisons. Topographical overlap between these 3 difference maps was finally tested by an AND conjunction. For example, the specific connectivity of cluster 1, compared with all other dmPFC clusters, was computed by the following conjunction: (cluster1–cluster2) AND (cluster1–cluster3) AND (cluster1–cluster 4).

In the MACM analysis, such specific connectivity patterns were only found for the rostroventral green cluster and the caudal-left yellow cluster (Fig. 5, top row). The rostroventral green cluster, more than all other dmPFC clusters, was connected to left PCC and bilateral IPC (area PGp), that is, regions that form the core of what is known as the default mode network (Buckner

et al. 2008). The caudal-left yellow cluster, in turn, was specifically connected to the (left) aMCC.

In the RSFC analysis, the rostroventral green cluster and the caudal-left yellow cluster showed similar functional connectivity (Fig. 5, bottom row) as in the specific MACM analyses. The rostroventral green cluster was specifically connected to the left PCC. The yellow cluster featured specific connectivity to left aMCC and—in addition to the MACM results—also the bilateral anterior insula.

Furthermore, RSFC analyses also revealed specific connectivity for the right-caudal red cluster and the rostrodorsal blue cluster: The right-caudal cluster was specifically connected to the right dlPFC, superior parietal cortex (7A, 7M; Scheperjans et al. 2008), intraparietal sulcus (hIP1, hIP3; Choi et al. 2006), IPC (PGa, PFm, PGp), dorsal PCC, and precuneus, middle temporal gyrus (MTG), and inferior temporal gyrus (ITG) as well as left cerebellum (lobule VIIa crus II). The rostrodorsal blue cluster further showed specific connectivity to left IFG, temporal pole and bilateral MTG, middle occipital gyri (MOG), and cerebelli (lobule VIIa right Crus I, left crus II).

It is noteworthy that RSFC yielded more distributed connections than MACM in all dmPFC clusters. RSFC thus also revealed more extensive specific connectivity patterns.

Functional Decoding of Clusters

After mapping the dmPFC subdivisions and delineating the ensuing clusters' connectivity, their functional profiles were determined based on cognitive terms from the BrainMap taxonomy (Fig. 6). For the sake of robustness, we focused on taxonomic associations that were significant in both the forward and reverse inference. Forward inference derives brain activity from a psychological term, whereas reverse inference derives a psychological term from brain activity (cf. methods). Behavioral domains (BDs) and paradigm classes (PCs) of all 4 clusters indicated a shared association with cognition as well as emotion. In line with this observation, the rostroventral green cluster, the rostrodorsal blue cluster, and the caudal-left yellow cluster showed common involvement in emotional discrimination tasks.

Figure 6. Functional decoding of individual dmPFC clusters. Each cluster's significant associations with psychological terms (Behavioral Domains and Paradigm Classes) from the BrainMap database (http://www.brainmap.org). Forward inference determines above-chance brain activity given the presence of a psychological term, whereas reverse inference determines the above-chance probability of a psychological term given observed brain activity. The *x*-axis indicates relative probability values.

Besides these commonalities in very broad functional domains, clusters were more specifically characterized by those taxonomic associations that were not found in any other dmPFC cluster. The caudal-right red cluster, unlike any other dmPFC cluster, was related to reward tasks. In contrast, the caudal-left dmPFC cluster 4 showed specific involvement in the visual-perceptual and spatial discrimination tasks. Rostrally in the dmPFC, the rostroventral green cluster featured specific involvement in language tasks, comprising semantic discrimination and covert reading. The rostrodorsal blue cluster revealed specific functional associations with different types of basic emotions.

Importantly, no commonalities were found for the left- and right-caudal cluster, except for the broad domains of emotion and cognition. Overlapping functional involvements were similarly rare between rostral and caudal clusters: only the blue and the yellow clusters were congruently related to film viewing. In contrast, both rostral clusters (blue and green) showed much more overlap in their functional profile. Rostral clusters related to social cognitive tasks, including theory of mind (e.g., perspective taking), episodic recall, and passive viewing. Please note that passive viewing may be a commonly co-labeled condition of social, emotional and cognitive tasks in the BrainMap database.

Discussion

The dmPFC subserves sophisticated manipulations of social information. Increasing evidence, however, suggests that the part of the human dmPFC related to high-level social cognition may contain functionally heterogeneous subregions (Amodio and Frith 2006; Gilbert, Gonen-Yaacovi, et al. 2010; Gilbert, Henson, et al. 2010). For example, different social cognition tasks, such as theory of mind, moral judgments, and empathy have been shown to recruit regionally distinct portions of the dmPFC (Mitchell et al. 2006; Gilbert, Henson, et al. 2010; Bzdok, Schilbach, et al. 2012). Therefore, the present study formally tested for heterogeneity in the dmPFC as defined by increased activation during complex social judgments that generalized across visual and auditory sensory input (Bzdok, Langner, et al. 2012; Hensel et al. forthcoming). By capitalizing on coactivation patterns in the BrainMap database (Fox and Lancaster 2002), the dmPFC seed was segregated into 4 clusters: 2 rostral ones (dorsal and ventral) and 2 caudal ones (left and right; Fig. 3). The rostral clusters, especially the rostroventral cluster, were strongly connected to the PCC and the IPC, components of the default mode network (DMN). Furthermore, both rostral clusters featured functional connections to the amygdala and hippocampus in the limbic system as well as functional associations with memory and social cognitive tasks. In contrast, the 2 caudal clusters were hemispherically divided and predominantly connected to the respective ipsilateral hemispheres. The caudal-right cluster was connected to a right-lateralized frontoparietal attentional network. The caudal-left cluster was connected to the left aMCC and bilateral anterior insulae, proposed to correspond to a salience network. Our results thus support a differentiation within the dmPFC as delineated by its response to higher-level social cognition by regionally distinct functional relations to limbic, attentional, and default mode networks as well as corresponding functional assignments.

Connections to the Limbic System

The 2 rostral clusters (green and blue) were congruently connected (across MACM and RSFC) to the left amygdala (assigned to LB and SF nuclei groups) and left hippocampus (assigned to

CA and HATA). In contrast, the caudal-left yellow cluster was congruently connected only to the left amygdala (assigned to LB) but not hippocampus. Importantly, white-matter bundles of the amygdala or fornix-carried bundles of the hippocampus were scarcely connected to the rostral or caudal dmPFC as measured by diffusion MRI (dMRI) in humans (Croxson et al. 2005). Another dMRI study in humans (Greicius et al. 2009) even concluded that the medial temporal lobe (including amygdala and hippocampus) and dmPFC appear not to have direct connections to the dmPFC.

Importantly, however, observed functional connections do not need to coincide with observed structural connections, and vice versa (cf. Greicius et al. 2009; Eickhoff et al. 2010). In fact, the present functional connectivity of the "rostral" dmPFC (green and blue clusters) with the amygdala and hippocampus is likely to be mediated by third-party regions, such as the PCC or RSC (cf. Morris et al. 1999; Lavenex et al. 2002; Kobayashi and Amaral 2003). This would be in line with our results as the only dmPFC cluster without significant connectivity to either amygdala or hippocampus (the red cluster) was also the only cluster without congruent connectivity to the PCC. In turn, the present functional connectivity of the "caudal" dmPFC (the yellow cluster) to the amygdala (i.e., LB and SF) may actually reflect existing axonal connections as well as a gradual rostro-caudal shift in cytoarchitecture. That is because the pregenual ACC (pACC), adjacent to the dmPFC/BA9, has frequently been observed to be axonally connected to the amygdala in animals (Devinsky et al. 1995). More specifically, tracer injection in the pACC of rhesus monkeys labeled the LB (in line with functional connectivity of the yellow cluster) in the amygdala but no area in the hippocampus (Vogt and Pandya 1987). We therefore note a convergence between earlier reports of axonal connectivity in monkeys and present reports of functional connectivity in humans. The caudal portion of the present dmPFC seed might thus relate to the known gradual rostro-caudal cytoarchitectonic change from the dmPFC to the pACC (Sarkissov 1955; Vogt and Pandya 1987). This shift from only functional amygdala connectivity of the "rostral" dmPFC to "both" functional and structural amygdala connectivity in the "caudal" dmPFC indicates a shift in our dmPFC seed between cytoarchitectonically different regions from the dmPFC proper (BA 9) to the pACC (p32).

Connections to the Default Mode Network

Of the 4 delineated clusters, the rostroventral green cluster was most consistently connected to the PCC and bilateral IPC, that is, core components of the default mode network. Neural activity in this network decreases during most tasks and increases during a small set of high-level tasks, including past, hypothetical, future, and navigational thinking (Buckner et al. 2008; Spreng et al. 2009; Bzdok, Langner, Schilbach, Jakobs, et al. 2013). First, only the green cluster was connected to the core nodes of this network (bilateral IPC and PCC, besides mPFC) congruently across MACM and RSFC. Second, only the green cluster exhibited connectivity to these network nodes when considering specific connectivity according to MACM (all nodes) and RSFC (bilateral PCC). The green cluster in the rostroventral dmPFC therefore showed the closest functional coupling with the DMN across task-related (MACM) and task-unrelated (RSFC) brain states.

This regionally specific dmPFC connectivity is relevant in light of the diverging literature with respect to the connectivity of the mPFC to the DMN. Neural activity related to the DMN has been discussed to be associated with the more "dorsal" mPFC (e.g., Weissman et al. 2006; Laird, Eickhoff, Li, et al. 2009; Pisapia

et al. 2012), more ventral mPFC (e.g., Schilbach et al. 2008; Mars et al. 2012), both (e.g., Shulman et al. 1997; Gusnard et al. 2001; Andrews-Hanna et al. 2010), or even with the neighboring ACC (Shulman et al. 1997; Laird, Eickhoff, Li, et al. 2009). In a recent fMRI study aimed at segregating the DMN (Bado et al. 2014), the dorsal mPFC was more active during emotional autobiographical recall, whereas the ventral mPFC was more metabolically active during rest. However, dmPFC versus vmPFC were noted to be preferentially connected to the lateral versus medial components of the DMN, respectively (Bzdok, Langner, Schilbach, Engemann, et al. 2013). Another DMN segregation using hierarchical clustering of fMRI data (Andrews-Hanna et al. 2010) associated the networks preferentially connected to the dmPFC versus vmPFC with thinking about the future versus present self. The authors further compared the functional correlations between 11 regions that composed their DMN. They reported that a region between dmPFC and vmPFC was connected to "all" DMN regions as graph-analytically measured by betweenness centrality. This middle mPFC region (on a ventrodorsal axis) is in close topographical proximity to the present rostroventral dmPFC cluster. Thus, previous and present results indicate that approximately the rostroventral green cluster yields the most consistent DMN connectivity across the medial prefrontal wall. Functional decoding of the rostroventral dmPFC also revealed implications in memory tasks, social cognition, and language processing. Indeed, previous quantitative meta-analyses showed the dmPFC to be consistently relate to memory, social, and language tasks (Binder et al. 2009; Spreng et al. 2009; Mar 2011). These results show that the most DMN-related cluster of the dmPFC is not only relevant for unconstrained cognition during rest, but also for some of the most sophisticated cognitive tasks. In sum, the present results agree with the currently scarce evidence for an important DMN node in the most frontopolar mPFC, most closely corresponding to the present rostroventral cluster. The functions of this DMN node seem to range from task-free to task-constrained processing.

Lateralization Effects in the Caudal dmPFC

In contrast to the rostral dmPFC, segregation in the caudal dmPFC (the caudal-right red cluster and the caudal-left yellow cluster) revealed hemisphere-specific connectivity patterns. The red cluster was connected to the left SFS according to MACM and RSFC and featured specific RSFC to a right-lateralized network composed of the right aMCC, dlPFC, IPC, precuneus, MTG, and ITG, as well as the left cerebellum. Although tracing studies in monkeys coincide with many of these connections (Carmichael and Price 1996; Barbas et al. 1999; Petrides and Pandya 2007), they did apparently not report or explicitly address hemispheric differences in "axonal connectivity." Nevertheless, "functional connectivity" of the (right-hemispheric) red cluster revealed clearly right-lateralized connections. In contrast, the (left-hemispheric) yellow cluster partly shared the connectivity pattern of the rostral dmPFC clusters, including connection to DMN areas. In addition, this cluster is specifically connected to the left aMCC (across MACM and RSFC) and bilateral anterior insula (RSFC). These findings match structural findings from dMRI in humans reporting enlarged anterior and midcingulate white-matter bundles in the left hemisphere (Gong et al. 2005; Wakana et al. 2007). Axons within this tract connect the dmPFC to the midcingulate cortex (Yeterian et al. 2012), which itself features axonal connections to the insula (Vogt and Pandya 1987; Augustine 1996; Saleem et al. 2007; van den Heuvel et al. 2009). In sum, functional connectivity of the caudal dmPFC reveals its

preferential involvement in ipsilateral neural networks. This difference in connectivity most likely explains the hemispheric division of the caudal dmPFC based on its whole-brain coactivation patterns.

Explanations for hemispheric lateralization range from interhemispheric inhibition to recruitment of contralateral regions during demanding tasks (Stephan et al. 2007). Hemispheric specialization may further subserve the isolation of simultaneously computed outputs (Chiarello and Maxfield 1996). To the best of our knowledge, no previous study has described the hemispherically distinct organization in the dmPFC. Yet, each caudal dmPFC cluster was specifically connected to the adjacent ipsilateral aMCC, which has been previously discussed in terms of lateralization. For example, during a dual task fMRI study, the left and right aMCC have been demonstrated to parallely encode the rewards of 2 separate tasks (Charron and Koechlin 2010). Moreover, left and right aMCC have been found to modulate ipsilateral brain regions in a task-dependent fashion (McIntosh and Lobaugh 2003; Stephan et al. 2003). When engaging participants in either verbal or visuospatial tasks on identical stimuli, analyses based on psychophysiological interactions revealed the left aMCC to be effectively connected to the left IFG during the verbal task, whereas the right aMCC was effectively connected to right IPL during a visuospatial task. This exemplifies how hemispheric specialization may allow the mediation between different task networks. Importantly, the present RSFC analyses indicate that, even in the absence of tasks, caudal dmPFC clusters are preferentially connected to networks within ipsilateral hemispheres. We thus corroborate absent lateralization in the rostral dmPFC (Gilbert, Gonen-Yaacovi, et al. 2010) and existing hemispherical specialization in the caudal dmPFC. The present lateralization in the caudal dmPFC might therefore indicate a functional integration of task-dependent as well as task-independent networks.

Interacting Networks in the dmPFC

The sets of brain regions beyond right and left aMCC, connected to caudal-right and caudal-left dmPFC, respectively, correspond to well-characterized neural networks (Dosenbach et al. 2007; Seeley et al. 2007): The frontoparietal connections of the (right-hemispheric) red cluster (SFG, dlPFC, IPC, and precuneus) largely correspond to a previously described executive network (Fox, Snyder, et al. 2005; Seeley et al. 2007). This frontoparietal network has been linked to attentional modulation of bottom-up processing of visuospatial information, especially in the right hemisphere (McIntosh et al. 1994; Corbetta and Shulman 2002; Corbetta et al. 2008; Thiebaut de Schotten et al. 2011). In contrast, aMCC and bilateral anterior insula, connected to the yellow cluster, have been conceptualized as a salience network (Seeley et al. 2007; Menon and Uddin 2010), potentially involved in interoceptive awareness (Critchley 2004), pain detection (Vogt 2005; Lamm et al. 2011), and empathy (Fan et al. 2011; Bzdok, Schilbach, et al. 2012). The general function of the salience network during these tasks may be the maintenance of pertinent cognitive sets and behavioral goals (Bush et al. 2002; O'Doherty et al. 2003; Dosenbach et al. 2007). Granger causality analyses further suggested the salience network to mediate between the mostly endogenously oriented DMN and the mostly exogenously oriented frontoparietal network during tasks (Sridharan et al. 2008; Uddin and Menon 2009; Menon and Uddin 2010; Chiong et al. 2013). In line with this assumption, task performance increases with causal influence from the aMCC on the dmPFC. In contrast, the reciprocal influence of the dmPFC on the aMCC relates to decreasing

performance (Wen et al. 2013). Concordantly, salience network lesions impair task performance combined with disinhibited DMN activation (Bonnelle et al. 2012).

The present results thus demonstrate the DMN, salience network, and right frontoparietal network to be connected to distinct dmPFC subregions. Specific DMN connectivity was found with the rostroventral green cluster, the frontoparietal network connected to the caudal-right (red) cluster and finally the caudal-left dmPFC cluster (yellow) features functional connections to both salience network and the DMN. These findings suggest a left-dominant salience processing in the dmPFC, conceivably modulating DMN activity to improve task performance. Taken together, the hemispheric specialization of the caudal dmPFC may allow an isolated computation of the mainly endogenously focused DMN and the mainly exogenously focused frontoparietal network. This might potentially be orchestrated by the salience network.

Understanding Previous Data in the Light of a New Functional Map

The dmPFC increases neural activity during unconstrained cognition as well as in numerous cognitive and emotional experimental settings (Laird, Eickhoff, Li, et al. 2009; Spreng et al. 2009; Mar 2011; Schilbach et al. 2012). Functional and anatomical alterations of the dmPFC have been further associated with diseases such as frontotemporal dementia, schizophrenia, and bipolar disorder (Schroeter et al. 2008; Minzenberg et al. 2009; Ellison-Wright and Bullmore 2010). Yet, previous evidence already indicated heterogeneous dmPFC regions to differentially respond to social, emotional, memory, and attentional tasks (Gilbert, Henson, et al. 2010). Additionally, separate quantitative meta-analyses on theory-of-mind tasks (ToMs), moral judgments, and empathic processing were associated with activity increases in heterogeneous dmPFC regions (Spreng et al. 2009; Bzdok, Schilbach, et al. 2012). These previous results indicate subregionally distinct dmPFC contributions even within the class of social cognitive processes. As far as we know, no currently available micro- or macroanatomical atlas provides topographical segregation of the dmPFC. The present connectivity-based parcellation thus provides a first basis to interpret such previous data by a more detailed dmPFC map.

As a post hoc analysis, we quantified the regional overlap of 3 previously published coordinate-based meta-analyses of theory of mind, moral judgments, and empathy (Bzdok, Schilbach, et al. 2012) with each of the 4 CBP-derived dmPFC clusters (Table 2).

This topographical comparison located meta-analytic convergence underlying theory of mind and moral judgments to the rostral green and blue dmPFC clusters, whereas empathy activations converged more caudally (predominantly in the left cluster) in the dmPFC. This agrees with the rostral dmPFC's

association with episodic memory and connectivity to the PCC and hippocampus as shown in the current work. We would argue that these findings reflect a likely basis for mental scene construction disregarding processing present sensory input predominantly in the green cluster (Buckner et al. 2008; Spreng and Grady 2010). Such hypothetical simulations based on episodic memory might be more relevant to theory of mind and moral cognition than empathy processes. Especially, the latter often involves present and thus embodiment-mediated experiences, such as emotional expressions or pain (Hein and Singer 2008; Lamm et al. 2011). In contrast, moral judgments involve retrieval, manipulation, and binding of abstract social knowledge for probabilistic predictions (Moll et al. 2005; Bar 2007). In line with this, moral judgments showed highest convergence in the rostroventral green cluster, which exhibited most selective DMN connectivity in addition to functional associations with episodic and semantic memory (Fig. 6). Furthermore, coordinate-based meta-analyses on theory of mind and autobiographical memory (Spreng et al. 2009) have reported maxima corresponding to the rostroventral dmPFC (green cluster).

Intriguingly, the maximum of dmPFC atrophy in frontotemporal dementia patients is likewise located in the rostroventral green cluster (Schroeter et al. 2008). In line with the functional profile of this dmPFC cluster, diagnostic criteria of frontotemporal dementia include early decline in social interpersonal conduct, loss of insight, and language impairments (Neary et al. 1998). In contrast to ToMs and moral judgments, empathy showed a relatively high overlap with the caudal red and yellow clusters.

Please note that only the yellow cluster featured connections to the left aMCC and anterior insulae (salience network), which is likewise consistently recruited in empathetic judgments (Fan et al. 2011; Bernhardt and Singer 2012; Bzdok, Schilbach, et al. 2012). Hence, the relatively high caudal dmPFC involvement during empathy tasks likely corresponds to the caudal-left cluster's axonal access to empathy-related circuits. Moreover, abnormal decrease of gray matter in these regions and the caudal-left dmPFC (Bora et al. 2010) or caudal bilateral dmPFC (Ellison-Wright and Bullmore 2010), has been frequently reported in schizophrenia and bipolar disorder patients. Therefore, the salience network connectivity of the caudal-left dmPFC may not only explain its role in emotional tasks, but also psychopathological disturbances such as psychosis (Palaniyappan and Liddle 2012).

In sum, the present dmPFC parcellation provides a novel framework for the interpretation of heterogeneous task activations and disease-related findings. Memory demanding (i.e., potentially mental scene related) social cognitive tasks such as theory of mind and moral judgments were found to predominantly recruit the rostroventral dmPFC, whereas the more affective empathy tasks were associated with more caudal-left dmPFC recruitment.

Table 2 DmPFC recruitment of distinct social tasks and their topographical overlap with individual connectivity-derived dmPFC clusters

	Theory of mind (1558 voxels in dmPFC)	Moral judgment (2527 voxels in dmPFC)	Empathy (108 voxels in dmPFC)
Caudal-right cluster (red)	0.00% (0 voxels)	0.00% (0 voxels)	12.04% (13 voxels)
Rostroventral cluster (green)	37.08% (589 voxels)	57.70% (1458 voxels)	3.70% (4 voxels)
Rostrodorsal cluster (blue)	58.22% (907 voxels)	20.06% (507 voxels)	49.07% (53 voxels)
Caudal-left cluster (yellow)	3.98% (62 voxels)	22.24% (562 voxels)	35.19% (38 voxels)

Percentage of dmPFC cluster involvement in 3 different social cognitive tasks: meta-analytic convergence underlying Theory of mind, moral judgment, and empathy (Bzdok, Schilbach, et al. 2012) were tested for topographical overlap with the dmPFC VOI of the present study. These overlapping voxels were further assigned to all clusters. To illustrate the dissociable subregions' contributions to each task, color highlights overlap between dmPFC cluster and meta-analytic maps beyond 10%.

Divergence Between Functional Connectivity Measures

Our analyses indicated that the delineated dmPFC clusters exhibited prominent differences between task-related and task-unrelated functional coupling patterns. This observation contrasts previous bimodal studies of seed regions, such as in the nucleus accumbens (Cauda et al. 2011), where MACM and RSFC largely conformed. That is, functional connectivity of the brain's task state (MACM) and of the brain's resting state (RSFC) were repeatedly shown to exhibited more similarities than dissimilarities in the interaction pattern with the rest of the brain but this was not true in the present study. The dmPFC thus suggests itself as a candidate region for mediating between neural systems that are typically more active and less active during task performance, respectively. This might be true although the dichotomic distinction of brain systems into so-called task-positive and task-negative components is increasingly recognized as oversimplified (cf. Golland et al. 2007; Zhang and Raichle 2010; Lamm et al. 2011). A potential mediation between fundamental (and perhaps even antagonistic) brain states is evidenced by the caudal-left yellow cluster's connectivity. During tasks (MACM) the yellow cluster featured strongest connectivity with the DMN, whereas during mind-wandering (RSFC) this cluster featured strongest connectivity to the putative salience network. This currently underappreciated neurobiological behavior is challenging to interpret given that the present data are purely "observational." Future research should capitalize on targeted "experimental" investigations using other methods to allow for its comprehensive characterization.

Conclusion

The present study systematically examined the heterogeneous nature of the dmPFC, involved in a multitude of high-level cognitive tasks, including social cognition in particular. Detailing the subdifferentiation of the dmPFC provided a segregation into 4 clusters of coherent whole-brain connectivity. Those located ventrally versus dorsally in the rostral dmPFC and left versus right in the caudal dmPFC. Both rostral clusters were functionally connected to the amygdala and hippocampus as well as involved in memory and social cognitive tasks. Furthermore, especially the rostroventral cluster was most strongly connected to the PCC and IPC. This corroborates previous evidence about this region as the most important DMN node in the prefrontal cortex. Caudally, the dmPFC was found to follow right- and left-hemispheric connectivity patterns that were connected to the so-called dorsal attention network and the salience network, respectively. We therefore demonstrate the existence of hemispheric specialization within the dmPFC and its differential implications in large-scale networks beyond the DMN. The present findings are particularly important in light of the dmPFC's frequent treatment as a unified region in the neuroimaging literature. Ultimately, the present mosaic view on dmPFC organization provides a useful neurobiological model for the interpretation of subregional findings.

Funding

Notes

References

Amft M, Bzdok D, Laird A, Fox P, Eickhoff S. Forthcoming. Definition and characterization of the extended default mode network. Brain Struct Funct.

Amodio DM, Frith CD. 2006. Meeting of minds: the medial frontal cortex and social cognition. Nat Rev Neurosci. 7:268–277.

Amunts K, Kedo O, Kindler M, Pieperhoff P, Mohlberg H, Shah NJ, Habel U, Schneider F, Zilles K. 2005. Cytoarchitectonic mapping of the human amygdala, hippocampal region and entorhinal cortex: intersubject variability and probability maps. Anat Embryol. 210:343–352.

Amunts K, Schleicher A, Burgel U, Mohlberg H, Uylings HB, Zilles K. 1999. Broca's region revisited: cytoarchitecture and intersubject variability. J Comp Neurol. 412:319–341.

Andrews-Hanna JR, Reidler JS, Sepulcre J, Poulin R, Buckner RL. 2010. Functional-anatomic fractionation of the brain's default network. Neuron. 65:550–562.

Ashburner J, Friston KJ. 2005. Unified segmentation. Neuroimage. 26:839–851.

Augustine JR. 1996. Circuitry and functional aspects of the insular lobe in primates including humans. Brain Res Rev. 22:229–244.

Bado P, Engel A, Oliveira-Souza R, Bramati IE, Paiva FF, Basilio R, Sato JR, Tovar-Moll F, Moll J. 2014. Functional dissociation of ventral frontal and dorsomedial default mode network components during resting state and emotional autobiographical recall. Hum Brain Mapp. 35:3302–3313.

Balsters JH, Laird AR, Fox PT, Eickhoff SB. 2014. Bridging the gap between functional and anatomical features of cortico-cerebellar circuits using meta-analytic connectivity modeling. Hum Brain Mapp. 35:3152–3169.

Bar M. 2007. The proactive brain: using analogies and associations to generate predictions. Trends Cogn Sci. 11:280–289.

Barbas H, Ghashghaei H, Dombrowski SM, Rempel-Clower NL. 1999. Medial prefrontal cortices are unified by common connections with superior temporal cortices and distinguished by input from memory-related areas in the rhesus monkey. J Comp Neurol. 410:343–367.

Bernhardt BC, Singer T. 2012. The neural basis of empathy. Annu Rev Neurosci. 35:1–23.

Binder JR, Desai RH, Graves WW, Conant LL. 2009. Where is the semantic system? A critical review and meta-analysis of 120 functional neuroimaging studies. Cereb Cortex. 19:2767–2796.

Biswal B, Yetkin FZ, Haughton VM, Hyde JS. 1995. Functional connectivity in the motor cortex of resting human brain using echo-planar MRI. Magn Reson Med. 34:537–541.

Bonin G. 1941. On encephalometry: a preliminary study of the brain of man, chimpanzee, and macaque. J Comp Neurol. 75:287–314.

Bonnelle V, Ham TE, Leech R, Kinnunen KM, Mehta MA, Greenwood RJ, Sharp DJ. 2012. Salience network integrity predicts default mode network function after traumatic brain injury. Proc Natl Acad Sci USA. 109:4690–4695.

Bora E, Fornito A, Yucel M, Pantelis C. 2010. Voxelwise meta-analysis of gray matter abnormalities in bipolar disorder. Biol Psychiatry. 67:1097–1105.

Brodmann K. 1909. Vergleichende Lokalisationslehre der Großhirnrinde. Leipzig (Germany): Barth.

Buckner RL, Andrews-Hanna JR, Schacter DL. 2008. The brain's default network: anatomy, function, and relevance to disease. Ann N Y Acad Sci. 1124:1–38.

Bush G, Vogt BA, Holmes J, Dale AM, Greve D, Jenike MA, Rosen BR. 2002. Dorsal anterior cingulate cortex: a role in reward-based decision making. Proc Natl Acad Sci USA. 99:523–528.

Byrne RW, Whiten A. 1988. Machiavellian intelligence: social expertise and the evolution of intellect in monkeys, apes, and humans. Oxford: Oxford University Press.

Bzdok D, Laird A, Zilles K, Fox PT, Eickhoff SB. 2012. An investigation of the structural, connectional and functional sub-specialization in the human amygdala. Hum Brain Mapp. 34:3247–3266.

Bzdok D, Langner R, Hoffstaedter F, Turetsky BI, Zilles K, Eickhoff SB. 2012. The modular neuroarchitecture of social judgments on faces. Cereb Cortex. 22:951–961.

Bzdok D, Langner R, Schilbach L, Engemann D, Laird AR, Fox PT, Eickhoff SB. 2013. Segregation of the human medial prefrontal cortex in social cognition. Front Hum Neurosci. 7:232.

Bzdok D, Langner R, Schilbach L, Jakobs O, Roski C, Caspers S, Laird A, Fox PT, Zilles K, Eickhoff SB. 2013. Characterization of the temporo-parietal junction by combining data-driven parcellation, complementary connectivity analyses, and functional decoding. Neuroimage. 81:381–392.

Bzdok D, Schilbach L, Vogeley K, Schneider K, Laird AR, Langner R, Eickhoff SB. 2012. Parsing the neural correlates of moral cognition: ALE meta-analysis on morality, theory of mind, and empathy. Brain Struct Funct. 217:783–796.

Carmichael S, Price J. 1994. Architectonic subdivision of the orbital and medial prefrontal cortex in the macaque monkey. J Comp Neurol. 346:366–402.

Carmichael ST, Price JL. 1996. Connectional networks within the orbital and medial prefrontal cortex of macaque monkeys. J Comp Neurol. 371:179–207.

Caspers S, Geyer S, Schleicher A, Mohlberg H, Amunts K, Zilles K. 2006. The human inferior parietal cortex: cytoarchitectonic parcellation and interindividual variability. Neuroimage. 33:430–448.

Cauda F, Cavanna AE, D'Agata F, Sacco K, Duca S, Geminiani GC. 2011. Functional connectivity and coactivation of the nucleus accumbens: a combined functional connectivity and structure-based meta-analysis. J Cogn Neurosci. 23:2864–2877.

Charron S, Koechlin E. 2010. Divided representation of concurrent goals in the human frontal lobes. Science. 328:360–363.

Chiarello C, Maxfield L. 1996. Varieties of interhemispheric inhibition, or how to keep a good hemisphere down. Brain Cogn. 30:81–108.

Chiong W, Wilson SM, D'Esposito M, Kayser AS, Grossman SN, Poorzand P, Seeley WW, Miller BL, Rankin KP. 2013. The salience network causally influences default mode network activity during moral reasoning. Brain. 136:1929–1941.

Choi HJ, Zilles K, Mohlberg H, Schleicher A, Fink GR, Armstrong E, Amunts K. 2006. Cytoarchitectonic identification and probabilistic mapping of two distinct areas within the anterior ventral bank of the human intraparietal sulcus. J Comp Neurol. 495:53–69.

Cieslik EC, Zilles K, Caspers S, Roski C, Kellermann TS, Jakobs O, Langner R, Laird AR, Fox PT, Eickhoff SB. 2013. Is there "one" DLPFC in cognitive action control? Evidence for heterogeneity from co-activation-based parcellation. Cereb Cortex. 23:2677–2689.

Clos M, Amunts K, Laird AR, Fox PT, Eickhoff SB. 2013. Tackling the multifunctional nature of Broca's region meta-analytically: co-activation-based parcellation of area 44. Neuroimage. 83C:174–188.

Corbetta M, Patel G, Shulman GL. 2008. The reorienting system of the human brain: from environment to theory of mind. Neuron. 58:306–324.

Corbetta M, Shulman GL. 2002. Control of goal-directed and stimulus-driven attention in the brain. Nat Rev Neurosci. 3:201–215.

Critchley HD. 2004. The human cortex responds to an interoceptive challenge. Proc Natl Acad Sci USA. 101:6333–6334.

Croxson PL, Johansen-Berg H, Behrens TE, Robson MD, Pinsk MA, Gross CG, Richter W, Richter MC, Kastner S, Rushworth MF. 2005. Quantitative investigation of connections of the prefrontal cortex in the human and macaque using probabilistic diffusion tractography. J Neurosci. 25:8854–8866.

Devinsky O, Morrell MJ, Vogt BA. 1995. Contributions of anterior cingulate cortex to behaviour. Brain. 118:279–306.

Diedrichsen J, Balsters JH, Flavell J, Cussans E, Ramnani N. 2009. A probabilistic MR atlas of the human cerebellum. Neuroimage. 46:39–46.

Dosenbach NU, Fair DA, Miezin FM, Cohen AL, Wenger KK, Dosenbach RA, Fox MD, Snyder AZ, Vincent JL, Raichle ME, et al. 2007. Distinct brain networks for adaptive and stable task control in humans. Proc Natl Acad Sci USA. 104:11073–11078.

Dunbar RIM. 1998. The social brain hypothesis. Evol Anthropol. 6:178–190.

Dunbar RIM, Shultz S. 2007. Evolution in the social brain. Science. 317:1344–1347.

Eickhoff SB, Bzdok D, Laird AR, Kurth F, Fox PT. 2012. Activation likelihood estimation meta-analysis revisited. Neuroimage. 59:2349–2361.

Eickhoff SB, Bzdok D, Laird AR, Roski C, Caspers S, Zilles K, Fox PT. 2011. Co-activation patterns distinguish cortical modules, their connectivity and functional differentiation. Neuroimage. 57:938–949.

Eickhoff SB, Jbabdi S, Caspers S, Laird AR, Fox PT, Zilles K, Behrens TE. 2010. Anatomical and functional connectivity of cytoarchitectonic areas within the human parietal operculum. J Neurosci. 30:6409–6421.

Eickhoff SB, Laird AR, Grefkes C, Wang LE, Zilles K, Fox PT. 2009. Coordinate-based activation likelihood estimation meta-analysis of neuroimaging data: a random-effects approach based on empirical estimates of spatial uncertainty. Hum Brain Mapp. 30:2907–2926.

Eickhoff SB, Paus T, Caspers S, Grosbras M-H, Evans AC, Zilles K, Amunts K. 2007. Assignment of functional activations to probabilistic cytoarchitectonic areas revisited. Neuroimage. 36:511–521.

Eickhoff SB, Schleicher A, Zilles K, Amunts K. 2006. The human parietal operculum. I. Cytoarchitectonic mapping of subdivisions. Cereb Cortex. 16:254–267.

Eickhoff SB, Stephan KE, Mohlberg H, Grefkes C, Fink GR, Amunts K, Zilles K. 2005. A new SPM toolbox for combining probabilistic cytoarchitectonic maps and functional imaging data. Neuroimage. 25:1325–1335.

Ellison-Wright I, Bullmore E. 2010. Anatomy of bipolar disorder and schizophrenia: a meta-analysis. Schizophr Res. 117:1–12.

Fan Y, Duncan NW, de Greck M, Northoff G. 2011. Is there a core neural network in empathy? An fMRI based quantitative meta-analysis. Neurosci Biobehav Rev. 35:903–911.

Forgy EW. 1965. Cluster analysis of multivariate data: efficiency versus interpretability of classifications. Biometrics. 21:768–769.

Fox DF, Raichle ME. 2007. Spontaneous fluctuations in brain activity observed with functional magnetic resonance imaging. Nat Rev Neurosci. 8:700–711.

Fox MD, Snyder AZ, Vincent JL, Corbetta M, Van Essen DC, Raichle ME. 2005. The human brain is intrinsically organized into dynamic, anticorrelated functional networks. Proc Natl Acad Sci USA. 102:9673–9678.

Fox PT, Laird AR, Fox SP, Fox PM, Uecker AM, Crank M, Koenig SF, Lancaster JL. 2005. BrainMap taxonomy of experimental design: description and evaluation. Hum Brain Mapp. 25: 185–198.

Fox PT, Lancaster JL. 2002. Opinion: mapping context and content: the BrainMap model. Nat Rev Neurosci. 3:319–321.

Geyer S. 2004. The microstructural border between the motor and the cognitive domain in the human cerebral cortex. Adv Anat Embryol Cell Biol. 174:I–VIII, 1–89.

Geyer S, Ledberg A, Schleicher A, Kinomura S, Schormann T, Burgel U, Klingberg T, Larsson J, Zilles K, Roland PE. 1996. Two different areas within the primary motor cortex of man. Nature. 382:805–807.

Geyer S, Schleicher A, Zilles K. 1999. Areas 3a, 3b, and 1 of human primary somatosensory cortex. Neuroimage. 10:63–83.

Gilbert SJ, Gonen-Yaacovi G, Benoit RG, Volle E, Burgess PW. 2010. Distinct functional connectivity associated with lateral versus medial rostral prefrontal cortex: a meta-analysis. Neuroimage. 53:1359–1367.

Gilbert SJ, Henson RN, Simons JS. 2010. The Scale of Functional Specialization within Human Prefrontal Cortex. J Neurosci. 30:1233–1237.

Golland Y, Bentin S, Gelbard H, Benjamini Y, Heller R, Nir Y, Hasson U, Malach R. 2007. Extrinsic and intrinsic systems in the posterior cortex of the human brain revealed during natural sensory stimulation. Cereb Cortex. 17:766–777.

Gong G, Jiang T, Zhu C, Zang Y, Wang F, Xie S, Xiao J, Guo X. 2005. Asymmetry analysis of cingulum based on scale-invariant parameterization by diffusion tensor imaging. Hum Brain Mapp. 24:92–98.

Greicius MD, Supekar K, Menon V, Dougherty RF. 2009. Resting-state functional connectivity reflects structural connectivity in the default mode network. Cereb Cortex. 19:72–78.

Gusnard DA, Akbudak E, Shulman GL, Raichle ME. 2001. Medial prefrontal cortex and self-referential mental activity: relation to a default mode of brain function. Proc Natl Acad Sci USA. 98:4259–4264.

Handl J, Knowles J, Kell DB. 2005. Computational cluster validation in post-genomic data analysis. Bioinformatics. 21:3201–3212.

Hartigan JA, Wong MA. 1979. A k-means clustering algorithm. Appl Stat. 28:100–108.

Hein G, Singer T. 2008. I feel how you feel but not always: the empathic brain and its modulation. Curr Opin Neurobiol. 18:153–158.

Hensel L, Bzdok D, Müller VI, Zilles K, Eickhoff SB. Forthcoming. Neural correlates of explicit social judgments on vocal stimuli. Cereb Cortex.

Hoffman MA. 2014. Evolution of the human brain: when bigger is better. Front Neuroanat. 8:15.

Holloway RL. 1968. The evolution of the primate brain: some aspects of quantitative relations. Brain Res. 7:121–172.

Holmes CJ, Hoge R, Collins L, Woods R, Toga AW, Evans AC. 1998. Enhancement of MR images using registration for signal averaging. J Comput Assist Tomogr. 22:324–333.

Humphrey NK. 1978. The social function of intellect. In: Bateson PPG, Hinde RA, editors. Growing points in ethology. Cambridge: Cambridge University Press. p. 303–317.

Jain AK, Murty MN, Flynn PJ. 1999. Data clustering: a review. ACN Comput Surveys. 31:264–323.

Jakobs O, Langner R, Caspers S, Roski C, Cieslik EC, Zilles K, Laird AR, Fox PT, Eickhoff SB. 2012. Across-study and within-subject functional connectivity of a right temporo-parietal junction subregion involved in stimulus-context integration. Neuroimage. 60:2389–2398.

Johansen-Berg H, Behrens TE, Robson MD, Drobnjak I, Rushworth MF, Brady JM, Smith SM, Higham DJ, Matthews PM. 2004. Changes in connectivity profiles define functionally distinct regions in human medial frontal cortex. Proc Natl Acad Sci USA. 101:13335–13340.

Kahnt T, Chang LJ, Park SQ, Heinzle J, Haynes JD. 2012. Connectivity-based parcellation of the human orbitofrontal cortex. J Neurosci. 32:6240–6250.

Kaufman L, Rousseeuw PJ. 1990. Finding groups in data: an introduction to cluster analysis. New York: J Am Statist Assoc.

Kelly C, Uddin LQ, Shehzad Z, Margulies DS, Castellanos FX, Milham MP, Petrides M. 2010. Broca's region: linking human brain functional connectivity data and non-human primate tracing anatomy studies. European J Neurosci. 32:383–398.

Kobayashi Y, Amaral DG. 2003. Macaque monkey retrosplenial cortex: II. cortical afferents. J Comp Neurol. 466:48–79.

Laird AR, Eickhoff SB, Fox PM, Uecker AM, Ray KL, Saenz JJ Jr, McKay DR, Bzdok D, Laird RW, Robinson JL, et al. 2011. The BrainMap strategy for standardization, sharing, and meta-analysis of neuroimaging data. BMC Res Notes. 4:349.

Laird AR, Eickhoff SB, Kurth F, Fox PM, Uecker AM, Turner JA, Robinson JL, Lancaster JL, Fox PT. 2009. ALE meta-analysis workflows via the brainmap database: progress towards a probabilistic functional brain atlas. Front Neuroinform. 3:23.

Laird AR, Eickhoff SB, Li K, Robin DA, Glahn DC, Fox PT. 2009. Investigating the functional heterogeneity of the default mode network using coordinate-based meta-analytic modeling. J Neurosci. 29:14496–14505.

Laird AR, Eickhoff SB, Rottschy C, Bzdok D, Ray KL, Fox PT. 2013. Networks of task co-activations. Neuroimage. 80:505–514.

Lamm C, Decety J, Singer T. 2011. Meta-analytic evidence for common and distinct neural networks associated with directly experienced pain and empathy for pain. Neuroimage. 54:2492–2502.

Lavenex P, Suzuki WA, Amaral DG. 2002. Perirhinal and parahippocampal cortices of the macaque monkey: projections to the neocortex. J Comp Neurol. 447:394–420.

Malikovic A, Amunts K, Schleicher A, Mohlberg H, Eickhoff SB, Wilms M, Palomero-Gallagher N, Armstrong E, Zilles K. 2007. Cytoarchitectonic analysis of the human extrastriate cortex in the region of V5/MT+: a probabilistic, stereotaxic map of area hOc5. Cereb Cortex. 17:562–574.

Mar RA. 2011. The neural bases of social cognition and story comprehension. Annu Rev Psychol. 62:103–134.

Mars RB, Neubert FX, Noonan MP, Sallet J, Toni I, Rushworth MF. 2012. On the relationship between the "default mode network" and the "social brain". Front Hum Neurosci. 6:189.

McIntosh AR, Grady CL, Ungerleider LG, Haxby JV, Rapoport SI, Horwitz B. 1994. Network analysis of cortical visual pathways mapped with PET. J Neurosci. 14:655–666.

McIntosh AR, Lobaugh NJ. 2003. Neuroscience. When is a word not a word? Science. 301:322–323.

Meila M. 2007. Comparing clusterings—an information based distance. J Multivar Anal. 98:873–895.

Menon V, Uddin LQ. 2010. Saliency, switching, attention and control: a network model of insula function. Brain Struct Funct. 214:655–667.

Mesulam MM. 1998. From sensation to cognition. Brain. 121:1013–1052.

Minzenberg MJ, Laird AR, Thelen S, Carter CS, Glahn DC. 2009. Meta-analysis of 41 functional neuroimaging studies of executive function in schizophrenia. Arch Gen Psychiatry. 66:811–822.

Mitchell JP. 2009. Social psychology as a natural kind. Trends Cogn Sci. 13:246–251.

Mitchell JP, Macrae CN, Banaji MR. 2006. Dissociable medial prefrontal contributions to judgments of similar and dissimilar others. Neuron. 50:655–663.

Moll J, Zahn R, de Oliveira-Souza R, Krueger F, Grafman J. 2005. Opinion: the neural basis of human moral cognition. Nat Rev Neurosci. 6:799–809.

Morris R, Petrides M, Pandya DN. 1999. Architecture and connections of retrosplenial area 30 in the rhesus monkey (Macaca mulatta). Eur J Neurosci. 11:2506–2518.

Muller VI, Cieslik EC, Kellermann TS, Eickhoff SB. 2014. Crossmodal emotional integration in major depression. Soc Cogn Affect Neurosci. 9:839–848.

Neary D, Snowden JS, Gustafson L, Passant U, Stuss D, Black S, Freedman M, Kertesz A, Robert PH, Albert M, et al. 1998. Frontotemporal lobar degeneration: a consensus on clinical diagnostic criteria. Neurology. 51:1546–1554.

Nichols T, Brett M, Andersson J, Wager T, Poline JB. 2005. Valid conjunction inference with the minimum statistic. Neuroimage. 25:653–660.

O'Doherty J, Critchley H, Deichmann R, Dolan RJ. 2003. Dissociating valence of outcome from behavioral control in human orbital and ventral prefrontal cortices. J Neurosci. 23:7931–7939.

Öngür D, Ferry AT, Price JL. 2003. Architectonic subdivision of the human orbital and medial prefrontal cortex. J Comp Neurol. 460:425–449.

Palaniyappan L, Liddle PF. 2012. Does the salience network play a cardinal role in psychosis? An emerging hypothesis of insular dysfunction. J Psychiatry Neurosci. 37:17–27.

Passingham RE. 1973. Anatomical differences between the neocortex of man and other primates. Brain Behav Evol. 7:337–359.

Petrides M, Pandya DN. 2007. Efferent association pathways from the rostral prefrontal cortex in the macaque monkey. J Neurosci. 27:11573–11586.

Petrides M, Tomaiuolo F, Yeterian EH, Pandya DN. 2012. The prefrontal cortex: comparative architectonic organization in the human and the macaque monkey brains. Cortex. 48:46–57.

Pisapia N, Turatto M, Lin P, Jovicich J, Caramazza A. 2012. Unconscious priming instructions modulate activity in default and executive networks of the human brain. Cereb Cortex. 22:639–649.

Poldrack RA. 2006. Can cognitive processes be inferred from neuroimaging data? Trends Cogn Sci. 10:59–63.

Raichle ME, MacLeod AM, Snyder AZ, Powers WJ, Gusnard DA, Shulman GL. 2001. A default mode of brain function. Proc Natl Acad Sci USA. 98:676–682.

Reetz K, Dogan I, Rolfs A, Binkofski F, Schulz JB, Laird AR, Fox PT, Eickhoff SB. 2012. Investigating function and connectivity of morphometric findings—exemplified on cerebellar atrophy in spinocerebellar ataxia 17 (SCA17). Neuroimage. 62:1354–1366.

Rilling JK, Insel TR. 1999. The primate neocortex in comparative perspective using magnetic resonance imaging. J Hum Evol. 37:191–223.

Rottschy C, Caspers S, Roski C, Reetz K, Dogan I, Schulz JB, Zilles K, Laird AR, Fox PT, Eickhoff SB. 2013. Differentiated parietal connectivity of frontal regions for "what" and "where" memory. Brain Struct Funct. 218:1551–1567.

Saleem KS, Kondo H, Price JL. 2007. Complementary circuits connecting the orbital and medial prefrontal networks with the temporal, insular, and opercular cortex in the macaque monkey. J Comp Neurol. 506:659–693.

Sarkissov SA. 1955. Architectonics of the human telencephalic cortex. Berlin (Germany): Springer.

Satterthwaite TD, Elliott MA, Gerraty RT, Ruparel K, Loughead J, Calkins ME, Eickhoff SB, Hakonarson H, Gur RC, Gur RE, et al. 2013. An improved framework for confound regression and filtering for control of motion artifact in the preprocessing of resting-state functional connectivity data. Neuroimage. 64:240–256.

Scheperjans F, Hermann K, Eickhoff SB, Amunts K, Schleicher A, Zilles K. 2008. Observer-independent cytoarchitectonic mapping of the human superior parietal cortex. Cereb Cortex. 18:846–867.

Schilbach L, Bzdok D, Timmermans B, Fox PT, Laird AR, Vogeley K, Eickhoff SB. 2012. Introspective minds: using ALE meta-analyses to study commonalities in the neural correlates of emotional processing, social & unconstrained cognition. PLoS One. 7:e30920.

Schilbach L, Eickhoff SB, Rotarska-Jagiela A, Fink GR, Vogeley K. 2008. Minds at rest? Social cognition as the default mode of cognizing and its putative relationship to the "default system" of the brain. Conscious Cogn. 17:457–467.

Schoenemann PT, Sheehan MJ, Glotzer LD. 2005. Prefrontal white matter volume is disproportionately larger in humans than in other primates. Nat Neurosci. 8:242–252.

Schroeter ML, Raczka K, Neumann J, von Cramon DY. 2008. Neural networks in frontotemporal dementia—a meta-analysis. Neurobiol Aging. 29:418–426.

Seeley WW, Menon V, Schatzberg AF, Keller J, Glover GH, Kenna H, Reiss AL, Greicius MD. 2007. Dissociable intrinsic connectivity networks for salience processing and executive control. J Neurosci. 27:2349–2356.

Semendeferi K, Armstrong E, Schleicher A, Zilles K, Van Hoesen GW. 2001. Prefrontal cortex in humans and apes: a comparative study of area 10. Am J Phys Anthropol. 114:224–241.

Semendeferi K, Lu A, Schenker N, Damasio H. 2002. Humans and great apes share a large frontal cortex. Nat Neurosci. 5:272–276.

Shulman GL, Fiez JA, Corbetta M, Buckner RL, Miezin FM, Raichle ME, Petersen SE. 1997. Common blood flow changes across visual tasks: II. decreases in cerebral cortex. J Cogn Neurosci. 9:648–663.

Smaers JB, Steele J, Case CR, Cowper A, Amunts K, Zilles K. 2011. Primate prefrontal cortex evolution: human brains are the extreme of a lateralized ape trend. Brain Behav Evol. 77:67–78.

Spreng RN, Grady CL. 2010. Patterns of brain activity supporting autobiographical memory, prospection, and theory of mind, and their relationship to the default mode network. J Cogn Neurosci. 22:1112–1123.

Spreng RN, Mar RA, Kim AS. 2009. The common neural basis of autobiographical memory, prospection, navigation, theory of mind, and the default mode: a quantitative meta-analysis. J Cogn Neurosci. 21:489–510.

Sridharan D, Levitin DJ, Menon V. 2008. A critical role for the right fronto-insular cortex in switching between central-executive and default-mode networks. Proc Natl Acad Sci USA. 105:12569–12574.

Stephan KE, Fink GR, Marshall JC. 2007. Mechanisms of hemispheric specialization: insights from analyses of connectivity. Neuropsychologia. 45:209–228.

Stephan KE, Marshall JC, Friston KJ, Rowe JB, Ritzl A, Zilles K, Fink GR. 2003. Lateralized cognitive processes and lateralized task control in the human brain. Science. 301:384–386.

Thiebaut de Schotten M, Dell'Acqua F, Forkel SJ, Simmons A, Vergani F, Murphy DG, Catani M. 2011. A lateralized brain network for visuospatial attention. Nat Neurosci. 14:1245–1246.

Tibshirani R, Walther G, Hastie T. 2001. Estimating the number of clusters in a data set via the gap statistic. J Roy Statist Soc B. 63:411–423.

Turkeltaub PE, Eickhoff SB, Laird AR, Fox M, Wiener M, Fox P. 2012. Minimizing within-experiment and within-group effects in activation likelihood estimation meta-analyses. Hum Brain Mapp. 33:1–13.

Uddin LQ, Menon V. 2009. The anterior insula in autism: underconnected and under-examined. Neurosci Biobehav Rev. 33:1198–1203.

Van den Heuvel MP, Mandl RC, Kahn RS, Hulshoff Pol HE. 2009. Functionally linked resting-state networks reflect the underlying structural connectivity architecture of the human brain. Hum Brain Mapp. 30:3127–3141.

Vogt BA. 2005. Pain and emotion interactions in subregions of the cingulate gyrus. Nat Rev Neurosci. 6:533–544.

Vogt BA, Pandya DN. 1987. Cingulate cortex of the rhesus monkey: II. cortical afferents. J Comp Neurol. 262:271–289.

Wakana S, Caprihan A, Panzenboeck MM, Fallon JH, Perry M, Gollub RL, Hua K, Zhang J, Jiang H, Dubey P, et al. 2007. Reproducibility of quantitative tractography methods applied to cerebral white matter. Neuroimage. 36:630–644.

Weissman DH, Roberts KC, Visscher KM, Woldorff MG. 2006. The neural bases of momentary lapses in attention. Nat Neurosci. 9:971–978.

Wen X, Liu Y, Yao L, Ding M. 2013. Top-down regulation of default mode activity in spatial visual attention. J Neurosci. 33: 6444–6453.

Yarkoni T, Poldrack RA, Nichols TE, Van Essen DC, Wager TD. 2011. Large-scale automated synthesis of human functional neuroimaging data. Nat Methods. 8:665–670.

Yeterian EH, Pandya DN, Tomaiuolo F, Petrides M. 2012. The cortical connectivity of the prefrontal cortex in the monkey brain. Cortex. 48:58–81.

Zhang D, Raichle ME. 2010. Disease and the brain's dark energy. Nat Rev Neurol. 6:15–28.

Zilles K, Amunts K. 2010. Centenary of Brodmann's map—conception and fate. Nat Rev Neurosci. 11:139–145.

Zu Eulenburg P, Caspers S, Roski C, Eickhoff SB. 2012. Meta-analytical definition and functional connectivity of the human vestibular cortex. Neuroimage. 60:162–169.